Cell Reports

Article

Metoclopramide treatment blocks CD93-signaling-mediated self-renewal of chronic myeloid leukemia stem cells

Graphical Abstract

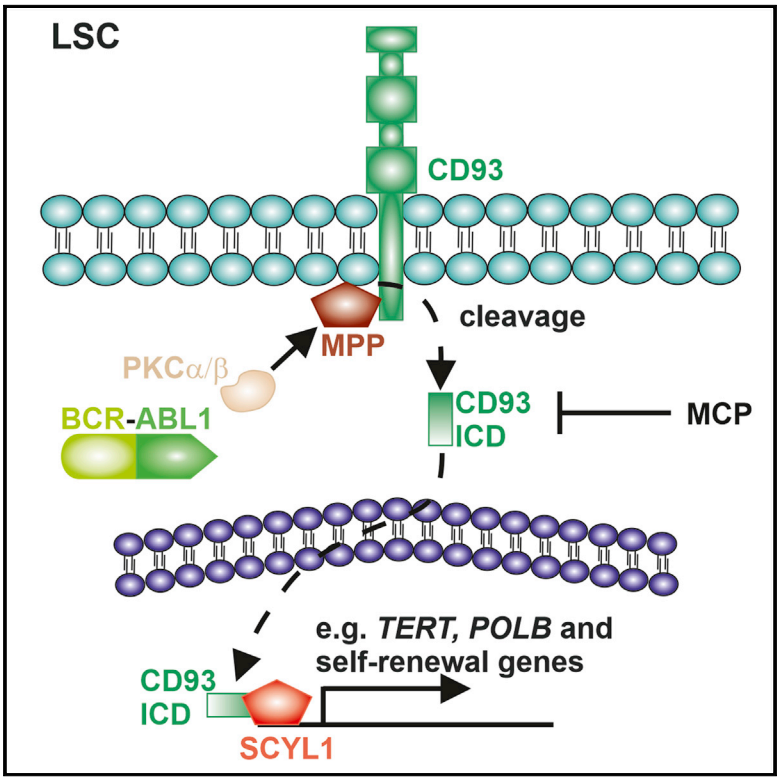

Highlights

- CD93 is a marker for leukemia stem cells (LSCs) in CML
- The intracellular domain of CD93 promotes stemness and self-renewal of CML LSCs
- The anti-emetic drug metoclopramide blocks CD93 signaling in LSCs

Authors

Carsten Riether, Ramin Radpour, Nils M. Kallen, ..., Christoph E. Albers, Gabriela M. Baerlocher, Adrian F. Ochsenbein

Correspondence

carsten.riether@dbmr.unibe.ch (C.R.), adrian.ochsenbein@insel.ch (A.F.O.)

In Brief

CD93 is a marker for LSCs in CML, but its broad expression on normal tissue hinders the development of CD93-targeting therapies. Riether et al. show that signaling via the intracellular domain of CD93 selectively promotes self-renewal of LSCs and that this process can be inhibited with the anti-emetic drug metoclopramide.

Riether et al., 2021, Cell Reports *34*, 108663
January 26, 2021
https://doi.org/10.1016/j.celrep.2020.108663

CellPress

Cell Reports

CellPress
OPEN ACCESS

Article

Metoclopramide treatment blocks CD93-signaling-mediated self-renewal of chronic myeloid leukemia stem cells

Carsten Riether,[1,2,9,*] Ramin Radpour,[1,2,8] Nils M. Kallen,[1,2,8] Damian T. Bürgin,[1,2,8] Chantal Bachmann,[1,2,3] Christian M. Schürch,[4] Ursina Lüthi,[1,2] Miroslav Arambasic,[1,2] Sven Hoppe,[5,6] Christoph E. Albers,[6] Gabriela M. Baerlocher,[2,7] and Adrian F. Ochsenbein[1,2,*]

[1]Department of Medical Oncology, Inselspital, Bern University Hospital, University of Bern, Bern, Switzerland
[2]Department for BioMedical Research (DBMR), University of Bern, Bern, Switzerland
[3]Graduate School of Cellular and Biomedical Sciences, University of Bern, Bern, Switzerland
[4]Baxter Laboratory for Stem Cell Biology, Department of Microbiology and Immunology, Stanford University School of Medicine, Stanford, CA, USA
[5]Wirbelsäulenmedizin Bern, Hirslanden Salem-Spital, Bern, Switzerland
[6]Department of Orthopedic Surgery and Traumatology, Inselspital, Bern University Hospital, University of Bern, Bern, Switzerland
[7]Department of Hematology and Central Hematology Laboratory, Inselspital, Bern University Hospital, University of Bern, Bern, Switzerland
[8]These authors contributed equally
[9]Lead contact
*Correspondence: carsten.riether@dbmr.unibe.ch (C.R.), adrian.ochsenbein@insel.ch (A.F.O.)
https://doi.org/10.1016/j.celrep.2020.108663

SUMMARY

Self-renewal is a key characteristic of leukemia stem cells (LSCs) responsible for the development and maintenance of leukemia. In this study, we identify CD93 as an important regulator of self-renewal and proliferation of murine and human LSCs, but not hematopoietic stem cells (HSCs). The intracellular domain of CD93 promotes gene transcription via the transcriptional regulator SCY1-like pseudokinase 1 independently of ligation of the extracellular domain. In a drug library screen, we identify the anti-emetic agent metoclopramide as an efficient blocker of CD93 signaling. Metoclopramide treatment reduces murine and human LSCs *in vitro* and prolongs survival of chronic myeloid leukemia (CML) mice through downregulation of pathways related to stemness and proliferation in LSCs. Overall, these results identify CD93 signaling as an LSC-specific regulator of self-renewal and proliferation and a targetable pathway to eliminate LSCs in CML.

INTRODUCTION

Leukemia stem cells (LSCs) have been characterized as the leukemia-initiating cells in acute myeloid leukemia (AML), chronic myeloid leukemia (CML), and other hematological neoplasms (Holyoake and Vetrie, 2017; Lapidot et al., 1994). In CML, LSCs are found in the majority of patients in the lineage-negative (Lin^-) $CD34^+CD38^-$ fraction of bone marrow (BM) cells, which is phenotypically similar to normal hematopoietic stem cells (HSCs) (Holyoake and Vetrie, 2017; Riether et al., 2015a). The introduction of BCR-ABL1-targeting tyrosine kinase inhibitors (TKIs) has revolutionized the treatment of CML. In chronic phase, CML patients often reach deep molecular remissions by treatment with first- or second-generation TKIs (Bhatia et al., 2003; Chu et al., 2011). A subgroup of these patients can successfully discontinue TKI therapy and maintain a treatment-free remission (Laneuville, 2017). However, TKI-insensitive LSCs persist in the majority of patients over a prolonged time period (Holyoake and Vetrie, 2017). These quiescent, self-renewing LSCs in the BM are the major cause of relapse after drug discontinuation or by the acquisition of mutations leading to TKI resistance (Holyoake and Vetrie, 2017; Jabbour et al., 2013; Savona and Talpaz, 2008).

CD93 ($C1qR_p$) is a C-type lectin-like type I transmembrane protein (Greenlee et al., 2008; Dean et al., 2000; Nepomuceno et al., 1997). Cleavage products of the intracellular domain (ICD) of CD93 have been detected in the cytoplasm of human monocytes after activation of protein kinase C (PKC) signaling (Bohlson et al., 2005a; Greenlee et al., 2009). The ICD of CD93 contains a nuclear localization signal that is thought to regulate gene expression by acting as a transcription factor in complex with other transcription factors (Cokol et al., 2000). CD93 is preferentially expressed on endothelial cells (ECs), platelets, myeloid cells, and early B cell precursors, but not lymphoid cells (Dean et al., 2000, 2001; Løvik et al., 2000; McKearn et al., 1985; Nepomuceno et al., 1997). In addition, CD93 is expressed on multipotent HSCs of the fetal liver and yolk sac (Huang and Auerbach, 1993) but is absent or very low on normal adult HSCs (Kinstrie et al., 2020). CD93 signaling is involved in many biological processes such as angiogenesis (Khan et al., 2017; Lorenzon et al., 2012; Petrenko et al., 1999), antibody production, and maintenance of long-lived plasma cells (Chevrier et al., 2009),

as well as the engulfment of apoptotic cells *in vivo* (Norsworthy et al., 2004). CD93 was identified as a marker for human CML LSCs that persist after TKI therapy (Kinstrie et al., 2020). In addition, CD93 signaling has been shown to induce proliferation and disease progression in AML LSCs carrying the MLL gene rearrangement (Iwasaki et al., 2015; Saito et al., 2010).

The ligands for CD93 are largely unknown. Initially, CD93 was thought to be a receptor for the complement factor C1q (Nepomuceno et al., 1997; Norsworthy et al., 2004). However, McGreal et al. reported that the CD93 receptor does not bind to C1q (McGreal and Gasque, 2002; McGreal et al., 2002). Instead, the EC-specific extracellular matrix protein multimerin 2 (MMRN2) has been recently identified as a potential ligand for CD93 and other receptors such as C-type lectin-domain-containing 14A (CLEC14A) and CD248 in HEK293 T cells (Khan et al., 2017).

Based on the documented expression of CD93 on LSCs, the aim of this study was to define its function in CML. CD93 is expressed on leukemia stem/progenitor cells (LSPCs), but not on more differentiated leukemia granulocytes. CD93 signaling promotes self-renewal and proliferation of LSCs, leading to disease progression in a murine CML model. RNA sequencing (RNA-seq) analysis reveals that CD93 signaling induces a stem-cell-maintenance- and proliferation-promoting gene expression program. Interestingly, the ICD of CD93 promotes gene transcription via the transcriptional regulator SCY1-like pseudo-kinase 1 (SCYL1) independently of ligand binding to the extracellular domain of CD93. Genetic ablation of CD93 signaling reduces the frequency of LSCs and prevents CML disease development in mice. Comparable to the results in murine CML, CD93 is expressed on human CML LSPCs, triggers the expression of genes involved in self-renewal and proliferation, and promotes colony formation *in vitro*. In a drug library screen, we identify metoclopramide (MCP) as an inhibitor of CD93-signaling in LSCs. MCP treatment reduces murine and human LSCs and prolongs survival of CML mice. These results identify CD93 as an important regulator of stemness of CML LSCs and a potential therapeutic target and the anti-emetic agent MCP as a drug that blocks CD93 signaling in CML.

RESULTS

CD93 signaling regulates self-renewal of LSCs

We analyzed the expression of CD93 on LSCs and leukemia progenitor cell populations in a murine retroviral transduction/transplantation CML model (Neering et al., 2007; Riether et al., 2015b). All LSC subsets (long-term LSCs [LT-LSCs], short-term LSCs [ST-LSCs], leukemia multipotent progenitor 1 [L-MPP1], and L-MPP 2) express CD93. In contrast, CD93 expression is lost on more differentiated Lin$^-$Sca-1$^-$c-kit^{hi} leukemic progenitors and leukemic GR-1$^+$ granulocytes (Figures 1A, 1B, and S1A). Similarly, all subpopulations of the Lin$^-$Sca-1$^+$c-kit^{hi} (LSK) fraction in the BM of naive mice (HSCs, multipotent progenitors [MPPs], and hematopoietic progenitor cells [HPCs]) expressed CD93 (Figure S1B). Lin$^-$c-kit^{hi} BM cells also express CD93, while more differentiated GR-1$^+$ granulocytes in the BM stain negative for CD93 (Figure S1B). Functionally, *Cd93*$^{-/-}$ LSCs form significantly fewer and smaller colonies in methylcellulose compared to controls (Figures 1C and 1D). The colony-forming capacity of LSCs is further reduced in secondary and tertiary replatings, suggesting that CD93 signaling promotes self-renewal of LT-LSCs (Figure 1E). In contrast, the clonogenic potential and cell numbers per colony of BL/6 and *Cd93*$^{-/-}$ LSKs are comparable (Figures 1F–1H). Overexpression of *Cd93* in BL/6 LSKs does not further increase their clonogenic potential *in vitro* (Figures S1C–S1F). The reduced colony-formation capacity of *Cd93*-deficient LSCs *in vitro* is independently confirmed in knockdown experiments using *Cd93*-targeting small hairpin RNA (shRNA) (Figures 1I–1L and S2A). Extreme limiting-dilution analysis (ELDA) reveals that knockdown of *Cd93* by shRNA reduces the frequency of LSCs in limiting-dilution experiments *in vitro* at by a factor of $\geq$100 (Figures 1K and 1L). These data suggest that CD93 signaling is required for self-renewal of LSCs, but not of HSCs.

CD93 signaling in LSCs promotes CML development *in vivo*

To study the functional relevance of CD93 signaling in LSCs *in vivo*, we transplanted BCR-ABL1-GFP transduced *Cd93*-proficient and deficient LSKs into nonirradiated BL/6 mice (BL/6 CML and *Cd93*$^{-/-}$ CML, respectively). Transplantation of BCR-ABL1-GFP$^+$ *Cd93*$^{-/-}$ LSKs into nonirradiated BL/6 recipient mice does not induce CML and results in a long-term survival, whereas *Cd93*-proficient BL/6 CML mice all die within 30 days (Figures 2A and 2B). No residual BCR-ABL1-GFP$^+$ cells are detected in blood, spleen, and BM of *Cd93*$^{-/-}$ CML mice by fluorescence-activated cell sorting (FACS) 90 days post-transplantation (data not shown). To determine residual disease with the most sensitive assay, we transplanted 5 × 10^6 BM cells of surviving primary *Cd93*$^{-/-}$ CML mice into lethally irradiated secondary recipients. All secondary recipients survive up to 90 days without any signs of leukemia (Figure 2C). In complementary experiments, we silenced *Cd93* in FACS-sorted BL/6 LSCs by shRNA before secondary transplantation into nonirradiated BL/6 mice (Figure 2D). sh*Cd93* knockdown results in an up to 70% reduction of *Cd93* mRNA compared to control scrambled (scr) shRNA-treated LSCs (Figure S2B). Similar to the results obtained in primary CML (Figures 2A and 2B), nonirradiated BL/6 mice injected with sh*Cd93* LSCs do not develop CML, survive long-term, and harbor no detectable disease 90 days after transplantation (Figures 2E and 2F; data not shown).

Since nonirradiated BL/6 mice transplanted with *Cd93*$^{-/-}$ CML did not develop the disease, we transplanted BCR-ABL1-GFP-transduced *Cd93*$^{-/-}$ and BL/6 LSKs into lethally irradiated BL/6 recipient mice. Theoretically, only a few functional LSCs are required to induce leukemia in lethally irradiated recipients (Neering et al., 2007). Indeed, BCR-ABL1-GFP-transduced *Cd93*$^{-/-}$ LSKs are able to engraft in lethally irradiated BL/6 recipients. However, the number of *Cd93*$^{-/-}$ LSCs in BM is reduced by a factor of 2 compared to BL/6 LSCs (Figure S2C).

To analyze the capacity of *Cd93*$^{-/-}$ LSCs to induce CML in immunocompetent hosts when injected at higher numbers, FACS-purified BL/6 and *Cd93*$^{-/-}$ LSCs from primary lethally irradiated CML mice were transplanted at titrated numbers into nonirradiated BL/6 mice, and survival was monitored (Figures 2G and 2H). All except one animal receiving BL/6 LSCs developed CML and succumbed to the disease (Figures 2G and 2H;

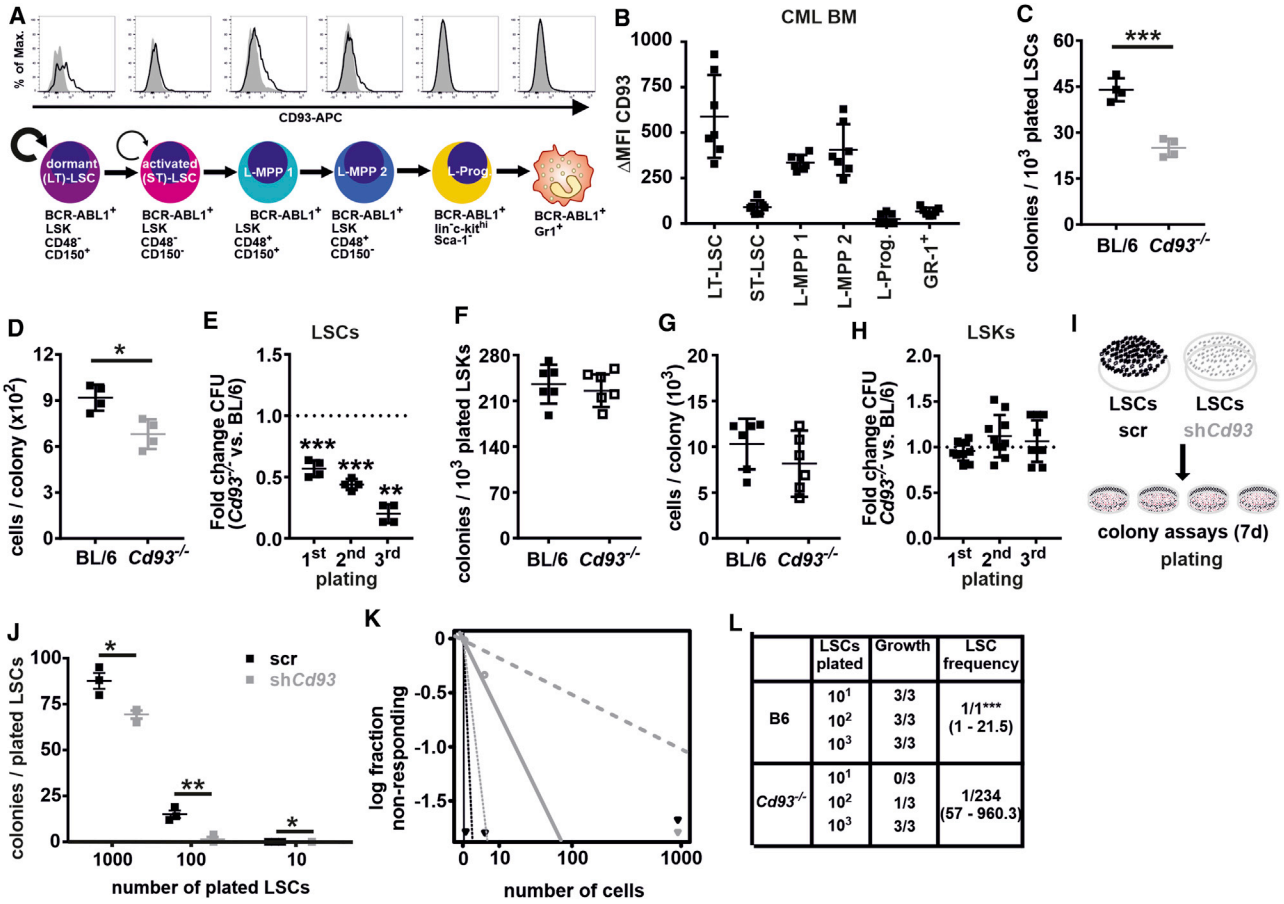

Figure 1. CD93 signaling regulates self-renewal of LSCs *in vitro*

(A and B) Representative histograms (A) and mean fluorescence intensities (MFIs) (B) for the expression of CD93 on LSCs, L-MPPs, leukemic progenitors, and leukemic granulocytes in the BM of CML mice. Isotype is depicted in gray and CD93 staining in black. ΔMFI: MFI staining − MFI isotype (n = 7 mice). Representative data from three independent experiments are shown.

(C) Myeloid colony-forming units (CFUs) per 10^3 plated BL/6 and *Cd93*$^{-/-}$ BM LSCs.

(D) Cells per colony.

(E) Serial replating capacity of BL/6 and *Cd93*$^{-/-}$ LSCs *in vitro* (n = 4 mice/group). One representative experiment out of two experiments is shown. For (C)–(E), significance was determined using a Student's t test (two-tailed).

(F) Myeloid CFUs per 10^3 plated BL/6 and *Cd93*$^{-/-}$ BM LSKs.

(G) Cells per colony from plated LSKs (n = 6 mice/group). One representative experiments out of two independent experiments is shown.

(H) Serial replating capacity of BL/6 and *Cd93*$^{-/-}$ LSKs *in vitro* (n = 9 mice/group). Pooled data from two independent experiments are shown. For (F)–(H), significance was determined using a Student's t test (two-tailed).

(I–L) Experimental setup. FACS-purified BL/6 LSCs from three different mice (n = 3 mice) were transduced with sh*Cd93* or scrambled (scr) control RNA particles and positively selected LSCs were plated in triplicates in methylcellulose at limiting dilution. (J) CFUs per 10^3 plated sh*Cd93*- or scr vector-transduced LSCs. Significance was determined using a Student's t test (two-tailed). (K and L) ELDA analysis. Significance was determined using a χ^2 test.

Data are represented as mean ± SD. *p < 0.05; **p < 0.01; ***p < 0.001.

data not shown). None of the mice receiving titrated numbers of *Cd93*$^{-/-}$ LSCs developed CML, and all recipient mice survived long-term, without signs of leukemia (data not shown). ELDA revealed that CD93 deficiency substantially reduced the number of functional LSCs capable of inducing leukemia in immunocompetent mice (Figure 2H).

To determine the contribution of CD93 signaling in host cells, BL/6 and *Cd93*$^{-/-}$ LSCs were additionally transferred into *Cd93*$^{-/-}$ recipient mice. While BL/6 LSCs induced leukemia in *Cd93*$^{-/-}$ mice with similar kinetics as in BL/6 mice, *Cd93*$^{-/-}$ LSCs were not able to promote leukemia development independently of the expression of CD93 on host cells (Figures S2D and S2E). These data indicate that CD93 signaling expands LSCs and promotes CML development in murine leukemia models.

CD93 signaling regulates self-renewal of LSCs independently of extracellular ligand binding

CD93 has previously been described as a receptor for the complement factor C1q, although these findings are controversial (Greenlee et al., 2009; McGreal and Gasque, 2002; McGreal et al., 2002). Heat inactivation destroys complement components (Soltis et al., 1979). To determine whether complement

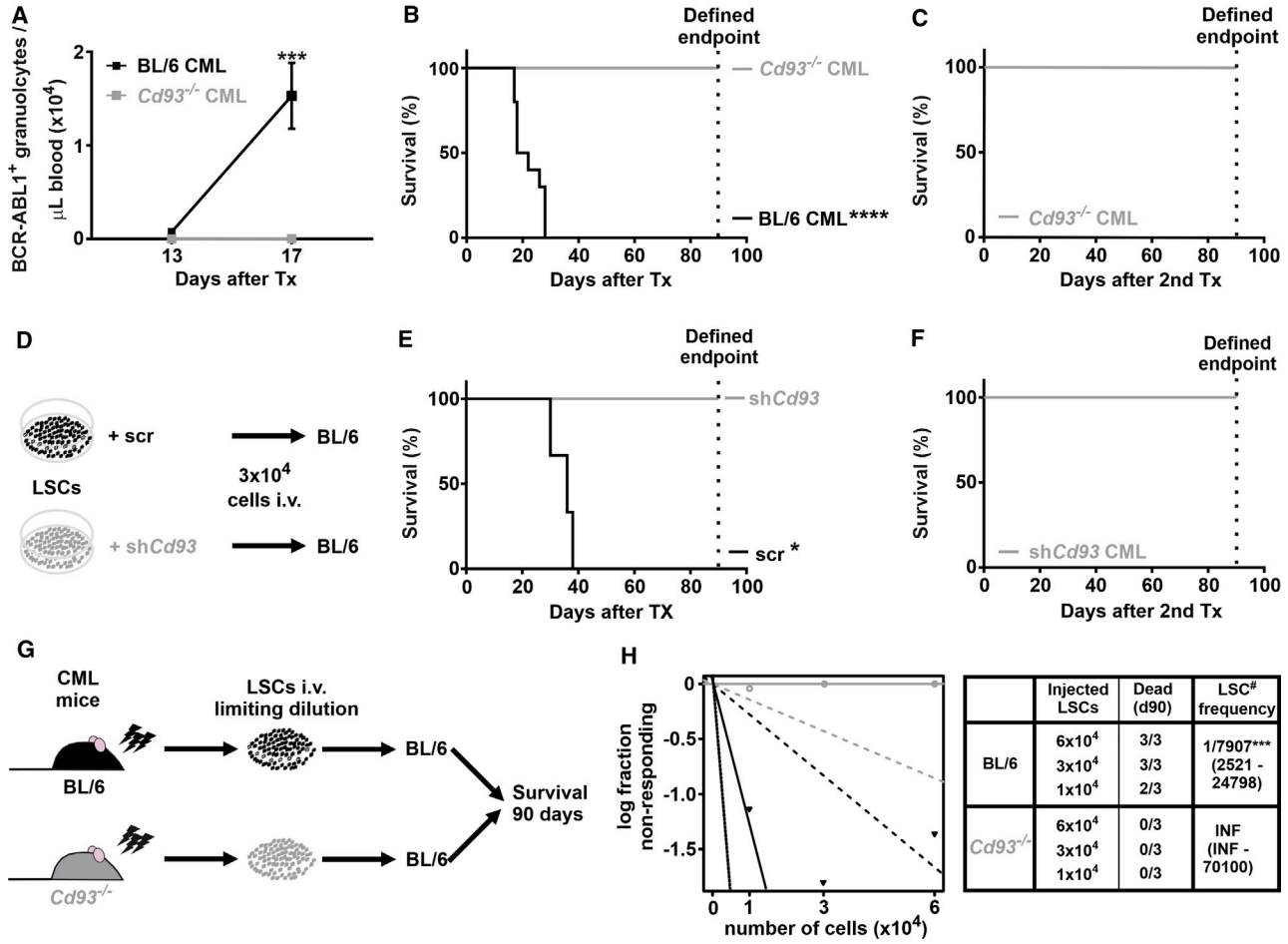

Figure 2. CD93 signaling in LSCs promotes CML development

(A and B) Numbers of BCR-ABL1-GFP$^+$ granulocytes/µl in blood (A) and Kaplan-Meier survival curves (B) resulting from primary transplantations of BCR-ABL1-GFP-transduced BL/6 (BL/6 CML) or *Cd93*$^{-/-}$ LSKs into naive, nonirradiated BL/6 recipients (n = 10 mice/group). Pooled data from two independent experiments are shown. Significance was determined using a two-way ANOVA followed by Bonferroni post-test (A) and a log-rank test (B).

(C) 5 × 10^6 whole BM cells from primary *Cd93*$^{-/-}$ CML mice 90 days after transplantation were transferred into lethally irradiated (2 × 6.5 Gy) secondary recipient mice, and survival was monitored (n = 10 mice).

(D–F) Pooled FACS-purified BL/6 LSCs were transduced with sh*Cd93* or scr control RNA lentiviral particles (n = 5 mice). shRNA-positive LSCs were selected by culture in puromycin-containing medium for 3 days and then transplanted into naive, nonirradiated BL/6 recipients, and survival was monitored (n = 6 mice per group). Pooled data from two independent experiments with n = 3 mice per group are shown. (D) Experimental setup. (E) Kaplan-Meier survival curves of transplanted mice (n = 6 mice per group). Pooled data from two independent experiments with n = 3 mice per group are shown. (F) 5 × 10^6 whole BM cells from primary sh*Cd93* CML mice 90 days after primary transplantation were injected into lethally irradiated (2 × 6.5 Gy) recipient mice (n = 6), and survival was monitored. Pooled data from two independent experiments with n = 3 mice per group are shown. Significance for (E) and (F) was determined using a log-rank test.

(G and H) BCR-ABL1-GFP-transduced BL/6 or *Cd93*$^{-/-}$ LSKs were transplanted into lethally irradiated (2 × 6.5 Gy) BL/6 recipients. After establishment of the disease, BL/6 or *Cd93*$^{-/-}$ LSCs were FACS purified and injected at limiting dilution into naive, nonirradiated BL/6 mice, and survival was monitored (n = 3 mice/dilution). (H) ELDA analysis. #, LSCs needed to induce CML in immunocompetent hosts. INF, infinity. One representative experiment out of two independent experiments is shown. Significance was determined by χ^2 test.

Data are represented as mean ± SD. *p < 0.05; ***p < 0.001; ****p < 0.0001.

factors, including C1q, trigger CD93 signaling in CML LSCs, we performed colony assays of *Cd93*-proficient and deficient LSCs in the presence of heat-inactivated (HI; no complement) and non-heat-inactivated (NHI; complement) fetal calf serum (FCS). BL/6 LSCs generate significantly more colonies than *Cd93*$^{-/-}$ LSCs independent of complement (Figure S2F).

To study whether CD93 signaling in LSCs relies on ligand binding to the extracellular domain of CD93, we generated retroviral vectors expressing either the complete murine *Cd93 (mCd93)* or a mutant with extracellular domain deletion of CD93 (*mCd93*^{intra}; Figures 3A and S3A–S3F). FACS analysis revealed that CD93 protein was detectable on *mCd93*-transduced *Cd93*$^{-/-}$ LSCs at a similar level as on empty vector (mock)-transduced BL/6 LSCs (Figure 3C). Interestingly, transduction of *Cd93*$^{-/-}$ LSCs with both *mCD93* and *mCd93*^{intra} restored colony formation of *Cd93*$^{-/-}$ LSCs *in vitro* (Figures 3D and 3E). These data indicate

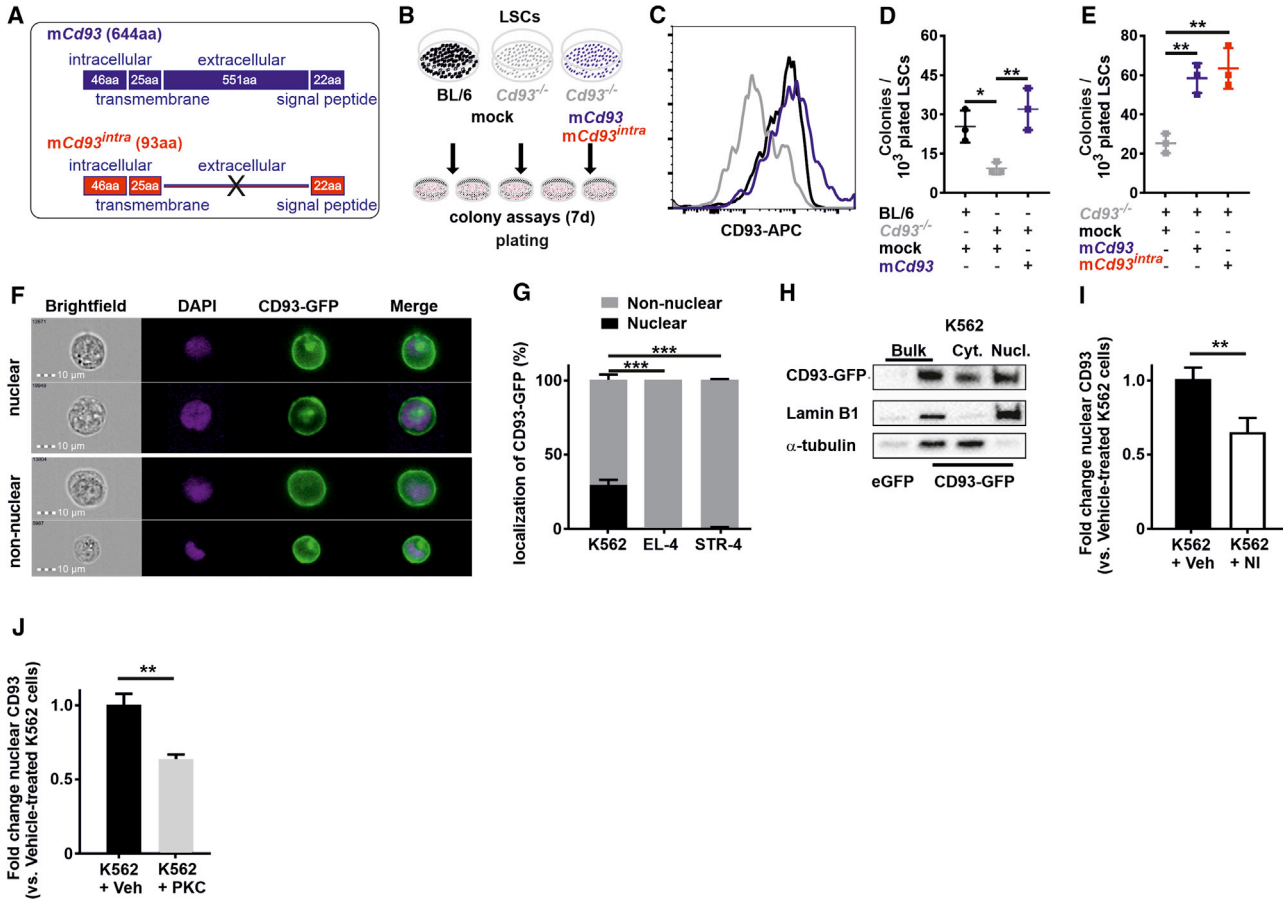

Figure 3. CD93 signaling regulates self-renewal of LSCs independent of extracellular ligand binding

(A–E) FACS-purified *Cd93*$^{-/-}$ CFP^{+} LSCs were transduced with an empty-GFP (mock)-, *mCd93*-GFP-, or *mCd93*^{intra}-GFP-expressing retroviral particles in triplicate. GFP^{+} LSCs were plated in methylcellulose in triplicate, and colony formation was assessed. (A) Domain structure of *mCd93* and *mCd93*^{intra}. (B) Experimental setup. (C) CD93 expression on CFP^{+} GFP^{+} LSCs (gray, *Cd93*$^{-/-}$ LSCs; black, BL/6 LSC: blue, m*Cd93* LSCs). (D) CFUs per 10^3 plated CFP^{+} GFP^{+} LSCs (n = 3 in triplicate/group). Significance was determined using a one-way ANOVA followed by Dunnett's post-test (versus *Cd93*$^{-/-}$ mock). (E) Colony formation of FACS-purified *Cd93*$^{-/-}$ CFP^{+} LSCs transduced with mock, *mCd93*, or *mCd93*^{intra} retrovirus. One representative experiment out of two independent experiments is shown. Significance was determined using a one-way ANOVA followed by Dunnett's post-test (versus *Cd93*$^{-/-}$ mock).

(F–I) The BCR-ABL-1-positive cell line K562 and the BCR-ABL-1-negative cell lines EL-4 and STR-4 were transfected with the mammalian expression plasmid pAcGFP1-N1-m*Cd93* encoding for AcGFP1-N1-m*Cd93* in triplicate. 48 h later, cells were analyzed for the subcellular localization of CD93. (F) Subcellular localization of CD93 in K562 cells analyzed by ImageStream. Two representative images of non-nuclear and nuclear CD93-GFP expression are shown. A minimum 1,200 GFP^{+} cells pre-sample were analyzed. (G) Percentage of nuclear and non-nuclear CD93-GFP localization analyzed by ImageStream. One representative experiment out of two independent experiments is shown. Significance was determined using a one-way ANOVA followed by Dunnett's post-test (versus K562). (H) Nuclear and cytosolic CD93-GFP determined by western blot. (I) Subcellular localization of CD93 in K562 cells treated with nilotinib (NIL; 70 µM) or vehicle for 72 h in triplicate. One representative experiment out of two independent experiments performed in triplicate is shown. Significance was determined using a Student's t test (two tailed).

(J) Subcellular localization of CD93 in K562 cells treated with PKC 20-28 (PKC; 50 µM) or vehicle for 72 h. One representative out of two independent experiments performed in triplicate is shown. Significance was determined using a Student's t test.

Data are represented as mean ± SD. **p < 0.01; ***p < 0.001.

that intracellular CD93 signaling promotes colony formation of LSCs independent of an extracellular ligand-receptor interaction.

The ICD of CD93 contains a nuclear localization signal that is thought to regulate gene transcription (Cokol et al., 2000). To investigate the subcellular localization of CD93 in CML, we cloned *mCd93* to the N terminus of a mammalian expression plasmid, AcGFP1 (pAcGFP1-N1-m*Cd93*), which leads to the expression of mCD93 protein fused to GFP (Figure S3G). pAcGFP1-N1-m*Cd93* was introduced into K562 CML cells (Chen, 1985), and the localization of the GFP-CD93 fusion protein was assessed by ImageStream (Figure 3F). The CD93-GFP fusion protein was detected at the cell membrane of all cells expressing pAcGFP1-N1-m*Cd93* (non-nuclear). Approximately 25% of these cells also expressed the fusion protein in the nucleus (Figures 3F and 3G). Cells transfected with pAcGFP1-N1-empty did not show a nuclear CD93-GFP signal (data not shown). These results are confirmed independently using a

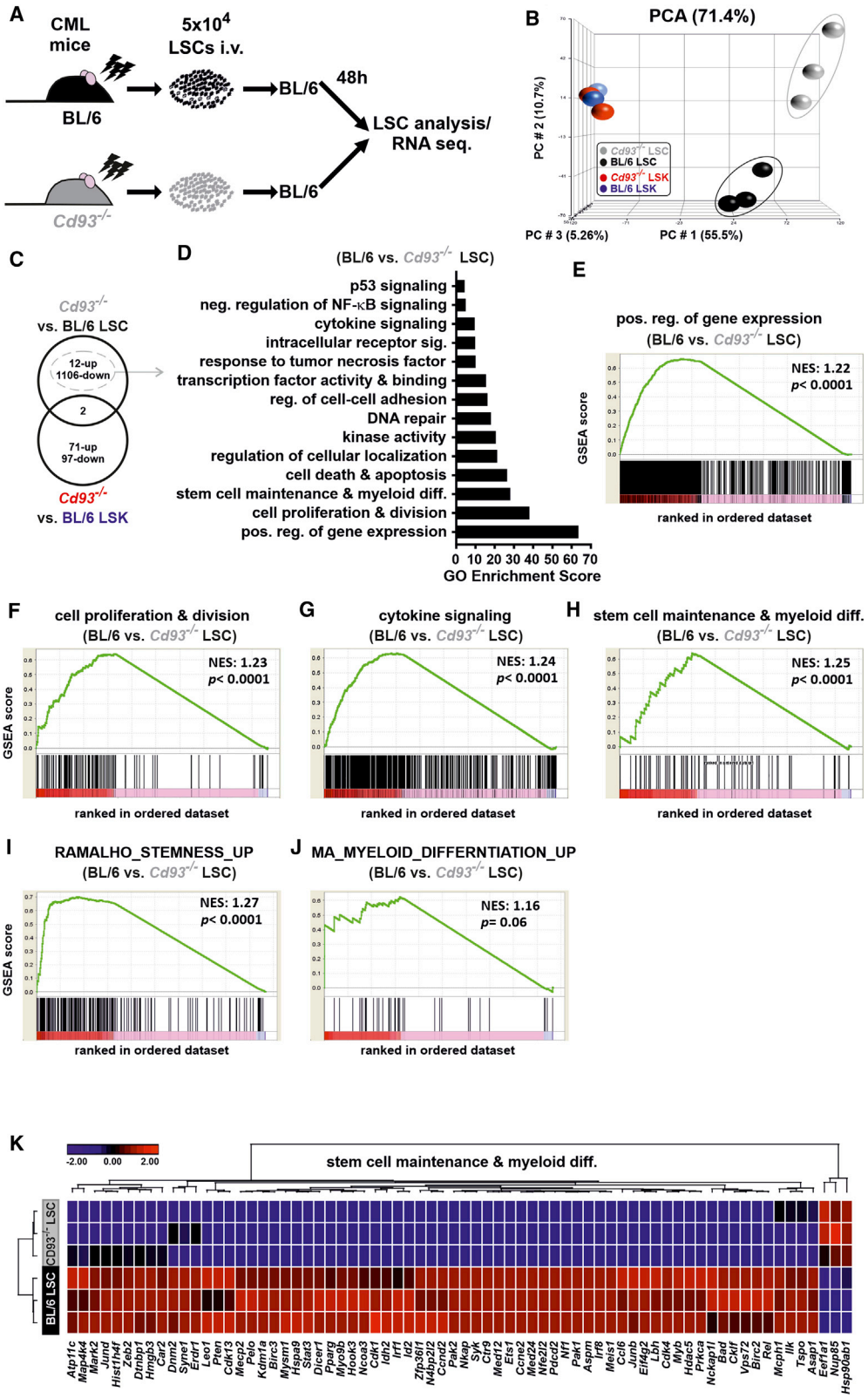

(legend on next page)

lentiviral expression vector encoding for AcGFP1-N1-m*Cd93* (pLVX-AcGFP1-N1-m*Cd93*) or AcGFP1-N1-empty (Figures S3H and S3I). To further confirm the nuclear localization of CD93, nuclear and cytosolic extracts of K562 cells transduced with AcGFP1-N1-m*Cd93* (CD93-GFP) or pAcGFP1-N1-empty (eGFP) were analyzed by western blot for the expression of GFP. CD93-GFP is detected in the cytosolic and in nuclear fraction of the cell extract (Figure 3H).

To investigate whether the subcellular distribution of CD93 is dependent on the expression of the BCR-ABL1 oncogene, we assessed the localization of CD93-GFP in BCR-ABL1-negative CD93-expressing EL-4 lymphoma (Gorer, 1950) and STR-4 endothelial BM cells (Aizawa et al., 1991) after transfection with pAcGFP1-N1-m*Cd93*. In contrast to BCR-ABL1-expressing K562 CML cells, the CD93-GFP fusion protein was detected at the cell membrane, but not in the nucleus of EL-4 and STR-4 cells (Figure 3G). Based on these findings, we hypothesized that the expression of nuclear CD93 is dependent on BCR-ABL1 activity. To analyze this, we inhibited BCR-ABL1 activity in K562 CML cells using half maximal inhibitory concentrations (IC_{50}) of the TKI nilotinib. Pharmacological blockade of BCR-ABL1 activity significantly reduced the nuclear localization of CD93-GFP compared to vehicle-treated K562 cells (Figure 3I). These findings were confirmed using an intracellular antibody staining combined with ImageStream analysis (Figures S4A and S4B). In addition, we overexpressed m*Cd93* in BL/6 LSCs. Overexpression of CD93 in LSCs did not result in increased clonogenic potential and did not affect their responsiveness to nilotinib treatment (Figures S4C–S4F).

In monocytes, the generation of CD93 ICD has been previously shown to depend on protein kinase C (PKC) activity to promote their phagocytic activity (Bohlson et al., 2005a; Greenlee et al., 2009). Thus, we addressed whether a pharmacological inhibitor of PKC-α/β activity affects the subcellular localization of CD93-GFP in CML cells by ImageStream. Incubation of K562 cells with PKC 20–28 at an IC_{50} concentration of 50 μM reduced ~40% of the subcellular localization of CD93 compared to vehicle-treated control cells (Figure 3J). Overall, these results demonstrate that nuclear localization of CD93 depends on PKC-α/β- and BCR-ABL1.

CD93 signaling triggers stem-cell-maintenance- and cell proliferation-promoting signaling pathways in CML LSCs

The nuclear localization of the ICD of CD93 in CML suggests that CD93 might act as a transcription factor and regulate gene expression. Thus, we performed RNA-seq analysis of BL/6 and *Cd93*$^{-/-}$ LSCs 48 h after transfer into nonirradiated secondary BL/6 recipients (Figure 4A). To investigate whether different gene expression profiles already exist in naive LSKs, we also included *Cd93*-proficient and deficient LSKs in the analysis. All samples had a similar number of reads (Figure S4G). BL/6 and *Cd93*$^{-/-}$ HSCs closely clustered together in the principal-component analysis (PCA), and only 170 genes were differently expressed. BL/6 and *Cd93*$^{-/-}$ LSCs clearly separated from LSKs based on the expression of the BCR-ABL1 oncogene (principal component 1 [PC1]). Importantly, BL/6 and *Cd93*$^{-/-}$ LSCs were very different from each other (Figure 4B, PC2 and PC3), as reflected by differential expression of 1,120 genes in *Cd93*$^{-/-}$ versus BL/6 LSCs (Figure 4C; Table S1). Of note, *Cd93*$^{-/-}$ LSKs shared only two differentially expressed genes with *Cd93*$^{-/-}$ LSCs (Figures 4C and S5A).

Gene Ontology (GO) analysis assigned the 1,120 differently expressed genes in *Cd93*$^{-/-}$ LSCs mainly into 14 different GO categories (Figure 4D). Gene set enrichment analysis (GSEA) revealed a significant downregulation of genes involved in promoting stem cell maintenance and myeloid differentiation, cell proliferation and survival, response to cytokine signaling, and gene expression (Figures 4E–4K). RNA-seq results were independently confirmed by qRT-PCR for a set of selected genes (Figure S5I). In contrast, GSEA of naive BL/6 and *Cd93*$^{-/-}$ HSCs did not reveal a dysregulation in these pathways (Figures S5C–S5H; Table S1). In summary, our data suggest that CD93 signaling triggers a defined stemness- and proliferation-associated gene expression signature in CML LSCs, but not in normal HSCs.

CD93 signaling regulates gene transcription in CML LSCs via Scyl1

To further determine the mechanism how CD93 affects gene expression in CML LSCs, we performed an *in silico* pathway analysis for proteins with a predicted physical interaction with CD93. The analysis identified six functional interaction partners for CD93. Among these six interaction partners, we identified one protein, SCYL1, with a reported role as a regulator of gene transcription (Figure 5A) (Burman et al., 2008). SCYL1 alias P105 was shown to interact directly with the highly charged juxta-membrane domain of the cytoplasmic tail of CD93 using a yeast-two-hybrid screen (Bohlson et al., 2005b). *Scyl1* was comparably expressed in BL/6 LSKs and BL/6 LSCs (Figure S5J). However, *Scyl1* expression was strongly reduced in *Cd93*$^{-/-}$ LSCs compared to BL/6 LSCs (Figure 5B). SCYL1 activated transcription of the telomerase reverse transcriptase (*Tert*) and DNA polymerase beta (*Polb*), two DNA polymerases that are overexpressed in many different cancer types with a reported role in the regulation of cell immortalization and tumorigenesis (Deville

Figure 4. CD93 triggers stemness- and proliferation-promoting genes in CML LSCs

(A) Experimental setup. BCR-ABL1-GFP-transduced BL/6 or *Cd93*$^{-/-}$ LSKs were transplanted into lethally irradiated BL/6 recipients. After establishment of disease, BL/6 LSCs or *Cd93*$^{-/-}$ LSCs were purified, and 5 × 10^4 LSCs were injected into naive BL/6 mice. 48 h later, LSCs were isolated, and gene expression was analyzed by RNA sequencing (RNA-seq).

(B) PCA of BL/6 and *Cd93*$^{-/-}$ LSKs (n = 2 mice/group) as well as BL/6 and *Cd93*$^{-/-}$ LSCs (n = 3 mice per group).

(C) Venn diagram showing up- and downregulated genes in *Cd93*$^{-/-}$ versus BL/6 LSCs compared to *Cd93*$^{-/-}$ versus BL/6 LSKs.

(D) GO analysis (BL/6 versus *Cd93*$^{-/-}$ LSCs). A GO enrichment score of ≥3 indicates significant changes in gene expression.

(E–J) GSEA of significantly enriched genes in BL/6 versus *Cd93*$^{-/-}$ LSCs.

(K) Heatmap of 70 differentially expressed genes promoting stem cell maintenance and myeloid differentiation.

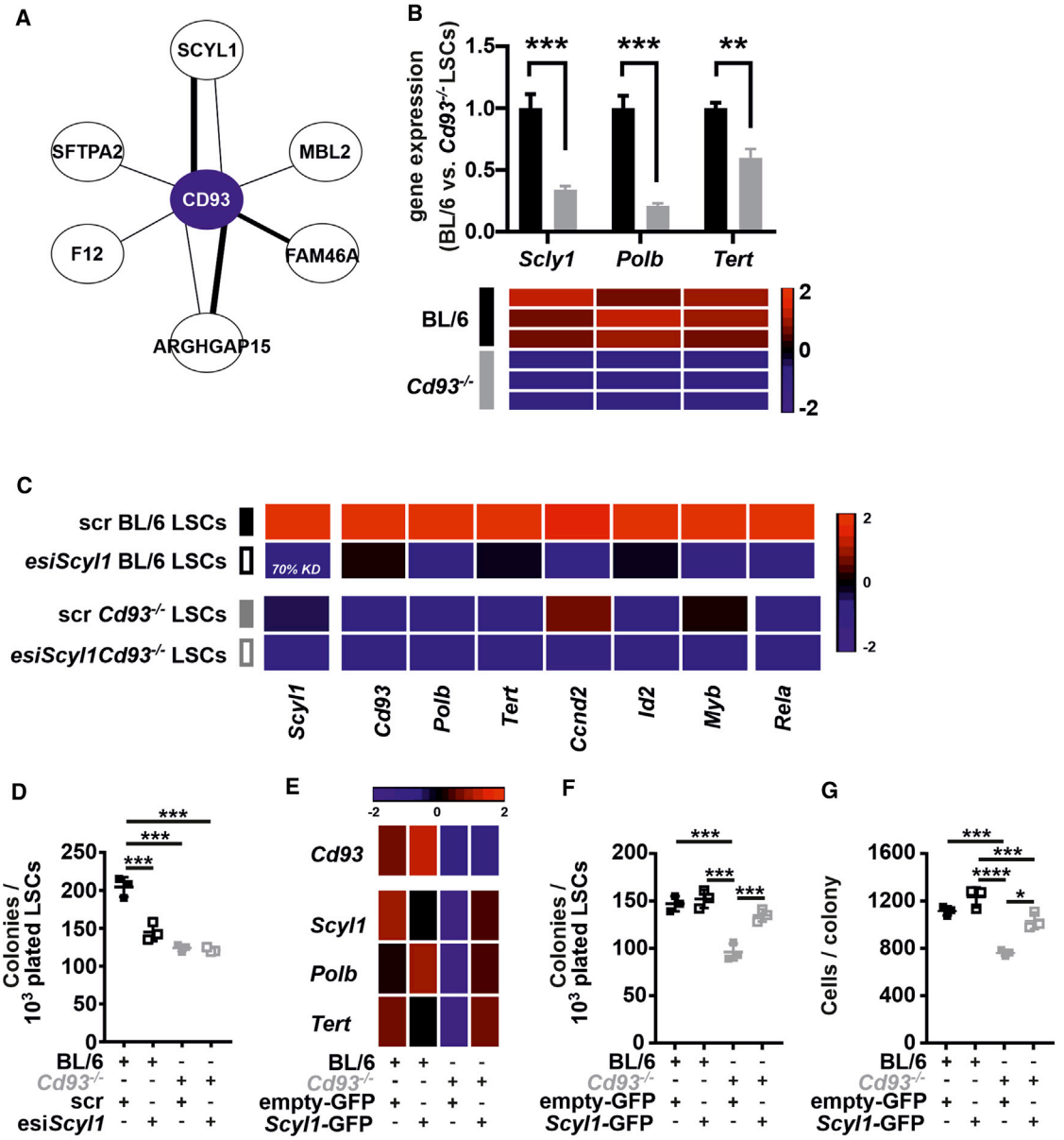

Figure 5. CD93 signaling triggers regulation of gene transcription in via SCYL1 in CML LSCs

(A) *In silico* analysis of predicted CD93 interaction partners using the GeneMANIA database (http://www.genemania.org/) (Warde-Farley et al., 2010).

(B) *Scyl1*, *Tert*, and *Polb* mRNA expression in *CD93*$^{-/-}$ and BL/6 LSKs and LSCs (n = 3 mice/group). Significance was determined using a Student's t test.

(C) Pooled FACS-purified BL/6 and *Cd93*$^{-/-}$ LSCs (n = 5 mice/group) were transduced with esi*Scyl1* or scr control esiRNA particles in triplicate, and gene expression was determined 48 h later. mRNA expression of *Cd93*, *Scyl1*, *Polb*, *Tert*, *CCnd2*, *Id2*, *Myb*, and *Rela* 48 after gene silencing of *Scyl1* by esiRNA. KD, knockdown efficiency (esiRNA versus scr).

(D) Colony formation. BL/6 and *Cd93*$^{-/-}$ LSCs were transduced esiScyl1 or scr control esiRNA particles as described in (C) followed by plating in methylcellulose in triplicate. Colony formation was assessed 7 days later. Significance was determined using a one-way ANOVA followed by Tukey's post-test.

(E–G) Pooled BCR-ABL1 CFP^{+} BL/6 and *Cd93*$^{-/-}$ LSCs (n = 5 mice/group) were transduced with a retrovirus expressing empty-GFP or *Scyl1*-GFP. 2 days later, CFP^{+}GFP^{+} LSCs were FACS purified, 10^3 cells were plated in methylcellulose in triplicate, and 10^4 cells were used for qRT-PCR analysis of *Scyl1*. Colony formation was assessed 7 days later. (E) *Scyl1*, *CD93*, *Tert*, and *PolB* mRNA expression, (F) colony formation, and (G) colony size of BL/6 and *Cd93*$^{-/-}$ LSCs expressing empty-GFP or *Scyl1*-GFP. Significance was determined using a one-way ANOVA followed by Tukey's post-test.

Data are represented as mean ± SD. **p < 0.01; ***p < 0.001.

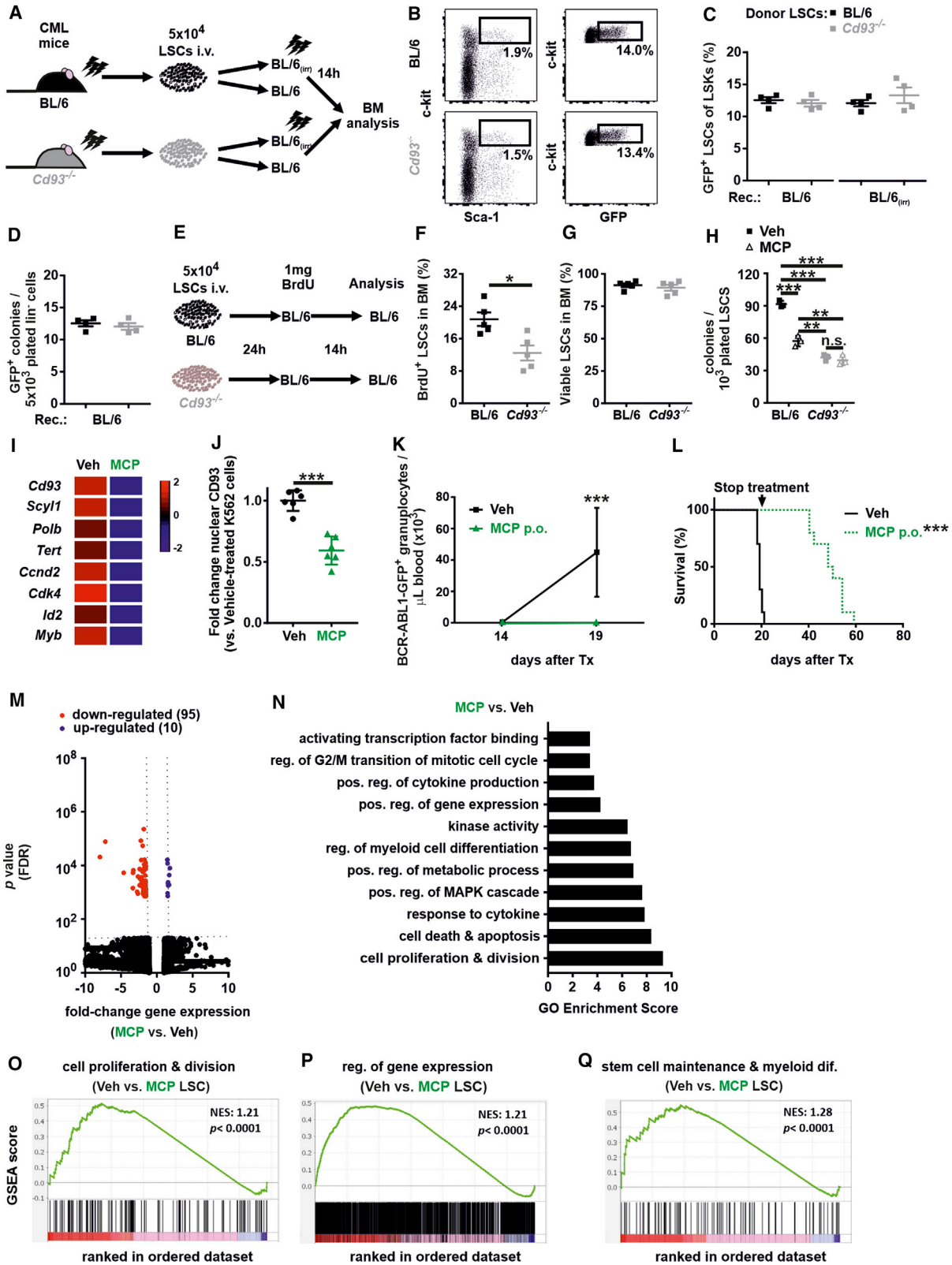

(legend on next page)

et al., 2009; Zhao et al., 2005). *Polb* and *Tert* expression was significantly reduced in *Cd93*$^{-/-}$ LSCs (Figure 5B). To analyze the role of *Scyl1* in CML LSCs, we silenced *Scyl1* in *Cd93*$^{-/-}$ and BL/6 LSCs by endoribonuclease-prepared siRNA (esiRNA). *esiScyl1* knockdown resulted in ~70% reduction of *Scyl1* mRNA in BL/6 LSCs compared to scr esiRNA-treated LSCs (Figure 5C). Silencing of *Scyl1* in BL/6 LSCs reduced the expression of the target genes *Polb and Tert* and selected genes related to self-renewal and proliferation (Figure 5C). Importantly, silencing *Scyl1* significantly reduced colony formation of BL/6, but not *Cd93*$^{-/-}$, LSCs *in vitro* (Figure 5D). Vice versa, overexpression of *Scyl1* in *Cd93*$^{-/-}$ LSCs increased mRNA expression of *Tert* and *PolB* and restored the clonogenic and differentiation potential of *Cd93*$^{-/-}$ LSCs to levels of empty-vector-transduced BL/6 LSCs (Figures 5E–5G). In contrast, overexpression of *Scyl1* in BL/6 LSCs did not affect *Tert* and *PolB mRNA* expression and their capacity to form colonies *in vitro* (Figure 5F, G). Overall, these findings indicate that the ICD of CD93 regulates gene transcription via *Scyl1* and its downstream genes, *Polb* and *Tert*, in CML LSCs.

CD93 signaling regulates proliferation of CML LSCs

Next, we analyzed the cellular processes by which CD93 signaling affects LSC function in more detail. Because CD93 is thought to be involved in cell adhesion and migration (Zhang et al., 2005), we first assessed the homing capacity of LSCs into the BM. Transplanted *Cd93*$^{-/-}$ and BL/6 LSCs similarly homed to the BM of lethally irradiated as well as nonirradiated BL/6 recipients (Figures 6A–6C). To confirm a similar frequency of functional LSCs in the BM 14 h after transplantation, total Lin$^-$ cells were plated in methylcellulose, and BCR-ABL1-GFP$^+$ colonies were assessed 7 days later. Lin$^-$ cells from mice receiving *Cd93*$^{-/-}$ and BL/6 LSCs formed similar numbers of BCR-ABL1-GFP$^+$ colonies (Figure 6D). These results indicate that CD93 signaling does not affect homing of LSCs *in vivo*.

Next, we assessed whether CD93 signaling affects proliferation and cell survival of LSCs. We injected *Cd93*-proficient and deficient LSCs into nonirradiated BL/6 mice (Figure 6E). Bromodeoxyuridine (BrdU)$^+$ incorporation is ~40% lower in *Cd93*$^{-/-}$ LSCs than in BL/6 LSCs, indicating a reduced proliferation of LSCs in the absence of CD93 (Figure 6F). Viability of BL/6 and *Cd93*$^{-/-}$ LSCs was comparable (Figure 6G). Overall, and in line with the data obtained in the gene enrichment analysis, these data suggest that *Cd93*$^{-/-}$ signaling promotes proliferation but does not affect apoptosis or homing of LSCs *in vivo*.

MCP blocks CD93 signaling and reduces LSC function *in vitro*.

To discover compounds that potentially block CD93 signaling, we performed a compound screen using the US Food and Drug Administration (FDA)-approved drug library V2 (Lago et al., 2019) (Table S2). *Cd93*-proficient and deficient LSCs were incubated overnight with 1 μM of the respective compounds, followed by plating in methylcellulose. Out of the 240 compounds tested, 10 compounds blocked CD93 signaling (Table S2). One interesting candidate that we identified in the

Figure 6. CD93 signaling induces proliferation of LSCs and is blocked by metoclopramide (MCP) treatment

(A) Experimental setup. FACS-purified BL/6 and *Cd93*$^{-/-}$ LSCs from lethally irradiated (2 × 6.5 Gy) primary CML mice were injected intravenously (i.v.) into naive as well as lethally irradiated BL/6 secondary recipient mice (n = 4 mice/group).

(B) Representative FACS plots of BCR-ABL1-GFP$^+$ BL/6 and *Cd93*$^{-/-}$ LSCs in the BM of naive BL/6 secondary recipients 14 h after transplantation mice (n = 4 mice/group).

(C) Frequencies of BCR-ABL1-GFP$^+$ BL/6 and *Cd93*$^{-/-}$ LSCs (n = 4 mice/group). Significance was determined using a Student's t test.

(D) BCR-ABL1-GFP$^+$ CFU capacity of total Lin$^-$ cells (n = 4 mice/group). Significance was determined using a Student's t test. For (A)–(D), one representative experiment out of two independent experiments is shown.

(E) Experimental setup. FACS-purified BL/6 and *Cd93*$^{-/-}$ LSCs from lethally irradiated primary CML mice were transplanted into naive BL/6 secondary recipients (n = 5 mice/group). After 24 h, animals were treated intraperitoneally (i.p.) with 1 mg BrdU and sacrificed 14 h later.

(F) Frequency of BrdU$^+$ LSCs (n = 5 mice/group). Significance was determined using a Student's t test.

(G) LSC viability as determined by viability dye staining (n = 5 mice/group). Significance was determined using a Student's t test. For (F) and (G), one representative experiment out of two independent experiments is shown.

(H) LSCs derived from BL/6 and *Cd93*$^{-/-}$ CML mice (n = 3 mice/group) were cultured overnight in duplicate with 1 μM MCP followed by plating in methylcellulose. Colony formation was assessed 7 days later. Significance was determined using a one-way ANOVA followed by Tukey's post-test. One representative out two independent experiments is shown.

(I) LSCs derived from BL/6 and *Cd93*$^{-/-}$ CML mice (n = 3 mice/group) were cultured in duplicate with 1 μM MCP, and mRNA expression of the indicated genes was determined 48 h later.

(J) K562 CML cells were transfected with the mammalian expression plasmid pAcGFP1-N1-*mCd93* encoding for AcGFP1-N1-*mCd93* in triplicate in the presence or absence of 1 μM MCP. After 72 h, cells were analyzed for the subcellular localization of CD93 by ImageStream. Pooled data of two independent experiments are shown. Significance was determined using a Student's t test.

(K and L) Numbers of BCR-ABL1-GFP$^+$ granulocytes/μl in blood (K) and Kaplan-Meier survival curves (L) resulting from primary transplantations of BCR-ABL1-GFP-transduced BL/6 LSKs into naive, nonirradiated BL/6 recipients. Starting at the day of transplantation, mice were treated p.o. with vehicle (Veh) or MCP (10 mg/kg; n = 10 mice/group) for a period of 20 days. Significance was determined by two-way ANOVA followed by Bonferroni post-test (K) and log-rank test (L). Pooled data from independent experiments are shown.

(M) Summary of the RNA-seq results. Volcano plot representation of differentially expressed genes in LSCs derived from MCP- versus vehicle-treated CML mice. Blue and red points mark the genes with significantly increased or decreased expression, respectively, in LSCs derived from MCP- versus vehicle-treated CML mice (false discovery rate [FDR] < 0.05). The x axis shows fold changes in gene expression, and the y axis shows the FDR p value of a gene being differentially expressed. Only genes with a fold change >−10 and <10 are shown.

(N) GO analysis (MCP versus vehicle). A GO enrichment score of ≥3 indicates significant ontology enrichment.

(O–Q) GSEA of LSCs derived from CML mice treated with vehicle or MCP (n = 3 mice/group).

Data are represented as mean ± SD. *p < 0.05; **p < 0.01; ***p < 0.001.

compound screen is the anti-emetic agent MCP. MCP treatment reduced colony formation of BL/6 LSCs to comparable levels as *Cd93*$^{-/-}$ LSCs without further affecting colony formation of *Cd93*$^{-/-}$ LSCs (Figure 6H). Comparable to blockade of CD93 signaling (Figure 4), MCP treatment reduced the expression of stem-cell-related genes as well as *Scyl1*, *Polb*, and *Tert* in BL/6 LSCs (Figure 6I). Overexpression of CD93 did not rescue the effect of MCP treatment on colony-formation capacity, indicating that the observed effect is dependent not on total CD93 expression but on the nuclear localization of the cleaved intracellular part of CD93 (Figure S6A).

To investigate whether MCP treatment directly affects CD93 signaling through modulation of the subcellular localization of CD93 in CML, we cultured CD93-GFP-transfected K562 cells in the presence or absence of 1 μM of MCP. CD93-GFP nuclear localization in MCP-treated K562 cells was significantly reduced compared to vehicle-treated cells (Figure 6J). Overall, these data suggest that MCP treatment reduces the function of CML LSCs through modulation of CD93 signaling.

MCP treatment prolongs survival of CML mice through downregulation of stem-cell-maintenance- and cell-proliferation-promoting signaling pathways in CML LSCs

To validate our findings *in vivo*, BL/6 mice were treated once daily with vehicle or 10 mg/kg MCP orally (p.o.) (Shalaby et al., 2013) starting at the day of leukemia transplantation for a period of 20 days. MCP treatment significantly delayed leukemia development and prolonged survival compared to the vehicle-treated group independent of the route of administration (Figures 6K and 6L).

To determine which signaling cascades are altered in LSCs upon MCP treatment, we performed RNA-seq analysis of LSCs isolated from the BM of CML mice that were previously treated with vehicle or MCP for 3 days starting at day 13 after CML induction. MCP treatment significantly reduced the leukemia load, as indicated by a decrease in BCR-ABL1-GFP^{+} granulocyte numbers in peripheral blood and spleen weight as well as lower numbers of LSCs in the BM (Figures S6B–S6D).

LSCs derived from CML mice treated with MCP clearly separated from control LSCs (Figure S6E). RNA-seq analysis identified 105 genes that are differentially expressed between the two treatment conditions (Figure 6M; Table S1). Similar to *Cd*93$^{-/-}$ LSCs (Figure 4C), the vast majority of genes in LSCs from MCP-treated CML mice were downregulated compared to controls. GO analysis assigned the 105 differently expressed genes mainly into 11 different GO categories (Figure 6N). GSEA revealed a significant downregulation of genes involved in promoting stem cell maintenance and myeloid differentiation, cell proliferation and survival, response to cytokine signaling, and gene expression (Figures 6O–6Q and S6F–S6H). These data suggest that MCP treatment, similar to blockade of CD93 signaling, reduces the expression genes associated with stemness and proliferation in LSCs.

CD93 is expressed on the surface and in the nucleus of primary human CML stem/progenitor cells

To determine the relevance of our findings for human CML, we analyzed mRNA expression of *CD93* and its downstream target, *SCYL1*, in BM, CD34^{+}CD38^{+} leukemia progenitors, and CD34^{+}CD38^{-} LSCs of chronic-phase CML patients using two publicly available microarray datasets (GSE4170 and GSE43754) (Gerber et al., 2013; Radich et al., 2006). We identified *CD93* and *SCYL1* expression in chronic-phase CML BM and CML stem/progenitor cells, but not in CD34^{+} stem/progenitor cells from healthy donors (Figures 7A and 7B).

Immunohistochemistry (IHC) of BM sections of CML patients revealed CD93 protein expression on CD34^{+} LSCs and BM vascular ECs (Table S3; Figures 7C and 7D). Similarly, CD93 was detected on BM Lin^{-}CD34^{+} and Lin^{-}CD34^{+}CD38^{-} CML stem/progenitor cells by FACS (Figures 7E and S6I). In line with previous findings (Iwasaki et al., 2015; Kinstrie et al., 2020; Saito et al., 2010), CD93 expression cannot be detected on the surface of stem and progenitor cells from healthy donor BM by FACS (Figure 7F).

Next, we addressed the subcellular distribution of CD93 in primary CD34^{+} CML stem/progenitor cells by ImageStream analysis. CD93 was detectable in the nucleus of primary CD34^{+} CML stem/progenitor cells (Figure 7G). In line with our findings derived in K562 CML cells, nilotinib treatment significantly reduced the frequency of cells expressing CD93 in the nucleus. In contrast, total CD93 expression was not affected by nilotinib treatment (Figure S6J). Overall, these data suggest that the localization of the cleaved intracellular part of CD93 is dependent of BCR-ABL1 activity (Figure 7H).

CD93 signaling regulates the colony-formation capacity of human CML stem/progenitor cells *in vitro*

To analyze the role of CD93 signaling, we treated FACS-purified Lin^{-}CD34^{+} CML stem/progenitor cells with *CD93*-targeting (si*CD93*) or control small interfering RNA (siRNA) (siCTRL) followed by plating in methylcellulose and gene expression analysis using qRT-PCR (Figures 7I–7L). Silencing of *CD93* significantly reduced the expression of stem cell self-renewal- (*ID2*, *MYB*, *PAK2*, and *REL*) and proliferation-promoting genes (*CK1*, *CDK4*, and *CCND2*), as well as genes associated with genome maintenance (*TERT* and *POLB*) (Figure 7J). These transcriptomic changes were functionally confirmed by a significantly reduced colony-formation capacity in the absence of CD93 signaling (Figure 7K). In contrast, CD93 signaling did not affect colony formation of normal BM stem/progenitor cells (Figure 7L). To determine the effect of MCP treatment on human CML, we incubated FACS-purified CD34^{+} BM CML stem/progenitor cells with two different concentrations of MCP followed by plating in methylcellulose. The plasma concentrations reached in humans treated with MCP is between 0.1 and 0.2 μM (Magueur et al., 1991). Comparable to blockade of CD93 signaling (Figure 7J), MCP treatment reduced the expression of *SCYL1*, *POLB*, and *TERT* in CML stem/progenitor cells (Figure 7M). In addition, colony formation in semi-solid cultures was significantly impaired by MCP treatment. This effect is maintained in subsequent replatings, even in the absence of MCP (Figure 7N). Importantly, the clonogenic potential of hematopoietic stem/progenitor cells from healthy donor BM was not affected by the treatment (Figures S6K–S6M).

We next investigated whether a treatment combination with MCP and nilotinib results in further reduction in colony formation

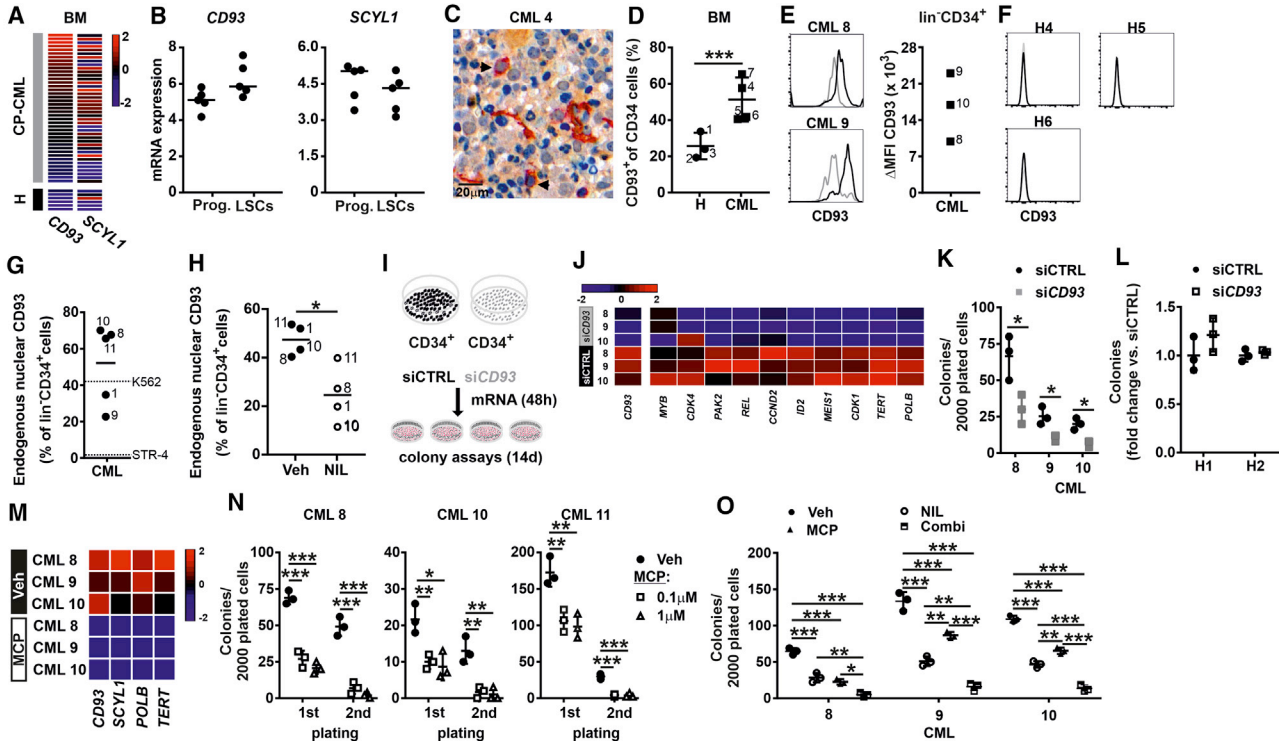

Figure 7. CD93 regulates colony-forming capacity of CD34⁺ BM stem/progenitor cells from CML patients *in vitro*

(A) A publicly available microarray dataset (GSE4170) that assessed gene expression profiles in CML was analyzed for *CD93* and *SCYL1* using the Gene Expression Omnibus GEO2R tool. Expression values of patients in chronic-phase CML (n = 42; green bars) and CD34⁺ stem/progenitor cells from healthy donor BM (n = 5; black bars) are shown.

(B) Expression of CD93 and SCYL1 mRNA in CD34⁺CD38⁺ leukemia progenitor cells (Prog.) and CD34⁺CD38⁻ LSCs from chronic-phase CML patients (GSE43754, n = 5 patients/group).

(C and D) CD93⁺CD34⁺ stem/progenitor cells in the BM of healthy donors (n = 3) and untreated CML patients (n = 4) were determined by immunohistochemistry (IHC) and cell morphology. (C) Representative IHC image for CD34 and CD93 in BM of CML (n = 4 CML patients). Slides were stained with a rabbit anti-human CD93 antibody, and staining was visualized with a 3,3'-diaminobenzidine (DAB) detection kit. Slides were subsequently counterstained and visualized with a mouse anti-human CD34 antibody and a red detection kit, respectively, followed by a counterstain with hematoxylin. CD93 is stained in brown and CD34 in red. Scale bar, 20 μm. Black arrows indicate CD93⁺CD34⁺ double-positive stem/progenitor cells. (D) Percentage of CD93-expressing CD34⁺ cells in CML and normal healthy donor BM (H) as analyzed by IHC. 145–328 CD34⁺ BM cells were analyzed per trephine biopsy. Significance was determined using a Student's t test (two tailed).

(E) Representative FACS histograms (left panel) and the MFI (right panel) of CD93 expression versus isotype control on Lin⁻CD34⁺ BM cells from CML patients. ΔMFI: MFI staining − MFI isotype.

(F) Histograms of CD93 expression on CD34⁺ BM stem/progenitor cells from healthy donors (H4–H6) as analyzed by FACS. Black lines, CD93 staining; gray lines, isotype controls.

(G) Subcellular localization of CD93 ICD in Lin⁻CD34⁺ CML stem/progenitor cells (CML 1 and 8–10). A minimum 5 × 10^3 cells pre-sample were analyzed. K562 and STR-4 cells served as positive and negative controls for nuclear CD93 expression, respectively. Numbers indicate patient IDs (Table S3).

(H) Subcellular localization of ICD of CD93 in Lin⁻CD34⁺ CML stem/progenitor cells (CML 1, 8, 10, and 11) treated with nilotinib (NIL; 5 μM) or vehicle for 24 h. A minimum of 10^3 cells per sample were analyzed. Numbers indicate patient IDs (Table S3). Significance was determined by paired Student's t test (two tailed).

(I–L) Lin⁻CD34⁺ BM stem/progenitor cells from CML patients 8–10 (Table S3) were treated with si*CD93* RNA (si*CD93*) or control siRNA (siCTRL) for 48 h in triplicate, followed by plating in methylcellulose or RNA isolation. (I) Experimental setup. (J) Heatmap for the expression of *CD93* and selected genes involved in self-renewal and cell proliferation in siCTRL versus si*CD93* cells. (K) Colony formation per 2,000 plated CD34⁺ BM stem/progenitor cells. Significance was determined using a Student's t test (two tailed). (L) Colony formation of 1,000 plated normal CD34⁺ BM stem/progenitor cells (H1 and H2) after silencing of CD93 by siRNA. Significance was determined using a Student's t test.

(M) CD34⁺ BM CML stem/progenitor cells (CML 8, 10, and 11) were treated 1 μM or vehicle overnight in triplicate followed by mRNA isolation. Heatmap of *CD93*, *SCYL1*, *POLB*, and *TERT* expression.

(N) CD34⁺ BM CML stem/progenitor cells (CML 8, 10, and 11) were treated with titrated concentrations of MCP or vehicle overnight in triplicate, followed by plating in methylcellulose. Colony formation of 2,000 plated cells for primary platings is shown. For secondary platings, 2 × 10^4 cells isolated from primary colony assays were replated in methylcellulose in the absence of the compound.

(O) CD34⁺ BM CML stem/progenitor cells (CML 8, 10 and 11) were treated with MCP (1 μM) and/or nilotinib (NIL; 5 μM) overnight in triplicate, followed by plating in methylcellulose. Colony formation of 2,000 plated cells for primary platings is shown. Significance was determined using a one-way ANOVA followed by Tukey's post-test.

Data are represented as mean ± SD. *p < 0.05; **p < 0.01; ***p < 0.001.

of CML stem/progenitor cells. We incubated FACS-purified $CD34^+$ BM CML stem/progenitor cells with 5 μM nilotinib and 1 μM MCP alone or in combination followed by plating in methylcellulose. The clonogenic potential in semi-solid cultures was significantly impaired by co-treatment compared to single treatments (Figure 7O). In summary, CD93 signaling expands human LSCs, a process that is efficiently blocked by MCP treatment.

DISCUSSION

The cancer stem cell (CSC) model suggests that leukemia may only be eradicated long-term by targeting disease-initiating and disease-maintaining LSCs (Holyoake and Vetrie, 2017; Riether et al., 2015a). LSCs frequently activate self-renewal and proliferation pathways to resist cytotoxic drugs and propagate the disease. These self-renewal pathways developed during evolution to maintain normal HSCs, the cell of origin for CML LSCs (Horne and Copland, 2017; Huntly and Gilliland, 2005). The selective elimination of LSCs requires the exploitation and targeting of unique signaling pathways that promote the self-renewal of LSCs, but not normal HSCs.

In the present study, we describe CD93 as an important regulator of self-renewal and proliferation of human and murine LSCs in CML. CD93 is expressed on many different cells, including ECs, plasma cells, B cell precursor cells, and hematopoietic cells (Dean et al., 2000, 2001; Løvik et al., 2000; McKearn et al., 1985; Nepomuceno et al., 1997). Interestingly, CD93 expression has been documented on CML LSCs and non-quiescent human MLL-rearranged AML LSCs, but not humans HSCs (Herrmann et al., 2020; Iwasaki et al., 2015; Kinstrie et al., 2020). In line with these findings, we document CD93 expression on all CML LSC subsets. CD93 deficiency in LSCs resulted in a severe impairment of proliferation and self-renewal of LSCs. As a consequence, CD93-deficient LSCs did not propagate the disease in immune-competent recipients. In contrast, although murine HSCs express CD93, self-renewal of HSCs was independent of CD93. *Cd93*$^{-/-}$ LSCs have a silenced gene expression signature, particularly for genes involved in cell proliferation and division as well as stem cell maintenance and myeloid differentiation. Out of the 1,120 genes differentially expressed between BL/6 and *Cd93*$^{-/-}$ LSCs, 1,108 genes were downregulated. Similarly, knockdown of *CD93* in human CML stem/progenitor cells reduced the expression of selected genes involved in stem cell self-renewal (*ID2*, *MYB*, *PAK2*, *MEIS1*, and *REL*) and proliferation (*CK1*, *CDK4*, and *CCND2*), confirming our results obtained in the murine CML model. These transcriptional changes resulted in a reduced colony-formation capacity *in vitro*, suggesting a similar regulation of CML stem/progenitor cells by CD93 in humans.

It is well documented that LSC self-renewal pathways are regulated by cell-autonomous signaling through interactions between LSCs and cells of the BM microenvironment or via altered intracellular signaling cascades mediated by the expression of the oncogene itself (Holyoake and Vetrie, 2017; Riether et al., 2015a). We demonstrate that LSCs regulate their function by promoting intracellular CD93 signaling via the ICD of CD93 independent of an extracellular ligand-receptor interaction. The formation of the CD93 ICD in leukemia cells was dependent on PKC activity. Similarly, in monocytes, the generation of CD93 ICD depends on PKC activity to promote their phagocytic activity (Bohlson et al., 2005a; Greenlee et al., 2009).

The ICD of CD93 contains a nuclear localization signal that is thought to regulate gene expression by acting as a transcription factor (Cokol et al., 2000). Genes involved in the regulation of gene expression were significantly silenced in LSCs in the absence of CD93 signaling. Our data suggest that signaling via the ICD of CD93 regulates gene expression in CML LSCs through interaction with the transcriptional regulator SCYL1 (Burman et al., 2008; Kato et al., 2002; Liu et al., 2000). SCYL1 has been previously identified to bind the ICD of CD93 through interaction with the juxta membrane domain of CD93 (Bohlson et al., 2005b). This signaling pathway is comparable to several other surface receptors regulating self-renewal in CML LSCs such as Notch, CD44, and others where the ICD fragment relocates to the nucleus and regulates gene transcription (Medina and Dotti, 2003; Okamoto et al., 2001; Schroeter et al., 1998). The ICDs of Notch1 and CD44 act as a co-transcription factors to trigger their own production and potentiate Notch1- and CD44 signaling (Okamoto et al., 2001; Sjöqvist et al., 2014). Similarly, CD93 deficiency resulted in a downregulation of SCYL1 suggesting a similar positive feedback loop for CD93 signaling. Similar to CD93, the nuclear localization of ICD of Notch1 and CD44 proteins is regulated by the activation of PKCs (Okamoto et al., 1999; Sjöqvist et al., 2014)

The promoters of both TERT and POLB belong to the promoter of TATA- or CAAT-less GC-rich genes, suggesting that some transcription factors might be involved in the transcriptional regulation of both polymerases (Kanamoto et al., 2004; Wick et al., 1999). As an example, SCYL1 binds to the promoters of DNA polymerases TERT and POLB, resulting in their transcription and activation (Deville et al., 2009; Zhao et al., 2005). TERT and POLB are active in normal stem cells and most cancer cells, including CSCs, but not in more differentiated cells (Deville et al., 2009; Zhao et al., 2005). POLB expression and activity are significantly higher in peripheral blood mononuclear cells (PBMCs) of CML patients compared to healthy donors (Canitrot et al., 2006). Similarly, telomerase expression and activity has been shown to increase in unfractionated BM cells of patients with CML during disease progression (Ohyashiki et al., 1997; Tatematsu et al., 1996; Verstovsek et al., 2003).

Our data indicate that silencing of *CD93* or *SCYL1* genes in LSCs reduces the expression of *TERT* and *POLB* in CML LSCs, resulting in the loss of proliferation and stem cell function. In line with these findings, studies on glioblastoma, neuroblastoma, breast cancer, prostate cancer, and pancreatic cancer documented increased telomerase activity in CSCs compared to non-CSCs. Inhibition of telomerase activity reduced self-renewal of CSCs, documenting a role of TERT in the regulation of stemness in CSCs (Castelo-Branco et al., 2011; Marian et al., 2010b, 2010a; Shay and Wright, 2010).

Due to its broad expression on different cell types, including ECs, targeting CD93 with antibodies, antibody conjugates, or chimeric antigen receptor (CAR)-T cells is difficult. However, the fact that the ICD of CD93 regulates gene expression and self-renewal exclusively in BCR-ABL1-transformed cells offers a selective targeting of this pathway in CML. We therefore

performed a compound screen using the FDA-approved drug library and identified 10 compounds that inhibit colony formation of BL/6, but not *Cd93*$^{-/-}$, LSCs. MCP was tested *in vitro* and *in vivo* and inhibited the expression of the target genes *SCYL1*, *TERT*, and *POLB* and colony formation of murine and human LSCs. In addition, MCP treatment, similar to blockade of CD93 signaling, prolonged survival of CML mice and reduced the expression of genes related to stemness and myeloid differentiation in LSCs. Because MCP is a very well-tolerated and cheap anti-emetic drug, its efficacy to eliminate LSCs in CML patients can be directly tested in clinical drug repurposing studies (e.g., in a TKI stop trial). In summary, CD93 signaling is a targetable pathway to eliminate LSCs in CML.

STAR★METHODS

Detailed methods are provided in the online version of this paper and include the following:

- KEY RESOURCES TABLE
- RESOURCE AVAILABILITY
  - Lead contact
  - Materials availability
  - Data and code availability
- EXPERIMENTAL MODEL AND SUBJECT DETAILS
  - Patient samples
  - Cell lines
  - Mice
- METHOD DETAILS
  - Study design
  - Antibodies
  - Colony assays
  - Gene silencing of CD93, Cd93 and Scyl1
  - Overexpression of mCd93
  - Overexpression of Scyl1
  - Sub-cellular localization of mCd93
  - ImageStream data acquisition and analysis
  - Sub-cellular fractionation and Western Blot
  - Immunohistochemistry (IHC)
  - High-throughput transcriptome analysis using next generation RNA sequencing (RNA-Seq)
  - RNA-Seq data analysis
  - Gene ontology (GO) and gene set enrichment analysis (GSEA).
  - qRT-PCR
  - CML model
  - LSPC and HSPC analysis
  - LSC homing experiments
  - BrdU incorporation *in vivo*
- QUANTIFICATION AND STATISTICAL ANALYSIS

SUPPLEMENTAL INFORMATION

Supplemental Information can be found online at https://doi.org/10.1016/j.celrep.2020.108663.

ACKNOWLEDGMENTS

We thank the staff of the FACSlab (Department for BioMedical Research [DBMR], University of Bern) and the TRU team (Institute of Pathology, University of Bern) for providing excellent technical assistance. This work was supported by the Swiss National Science Foundation (grants 31003A_149768 and 310030B_13313 to A.F.O. and grant 310030_179394 to C.R.), the Cancer League of the Canton of Berne, the Sassella Foundation, the Olga Mayenfisch Stiftung, and the Fondazione per la ricerca sulla trasfusione e sui trapianti.

AUTHOR CONTRIBUTIONS

Conceptualization, C.R. and A.F.O.; methodology, R.R., N.M.K., D.T.B., C.B., C.M.S., U.L., and M.A.; investigation, R.R., N.M.K., D.T.B., C.B., C.M.S., U.L., and M.A.; writing – original draft, C.R. and A.F.O.; writing – review & editing, all authors; resources, S.H., C.E.A., and G.M.B.; supervision, C.R. and A.F.O.

DECLARATION OF INTERESTS

The authors declare no competing interests. C.R. and A.F.O. are inventors on patent EP 19207529.9 submitted by University of Bern that covers CD93 inhibitors for the treatment of cancer.

Received: May 7, 2020
Revised: November 20, 2020
Accepted: December 28, 2020
Published: January 26, 2021

REFERENCES

Aizawa, S., Yaguchi, M., Nakano, M., Inokuchi, S., Handa, H., and Toyama, K. (1991). Establishment of a variety of human bone marrow stromal cell lines by the recombinant SV40-adenovirus vector. J. Cell. Physiol. *148*, 245–251.

Bhatia, R., Holtz, M., Niu, N., Gray, R., Snyder, D.S., Sawyers, C.L., Arber, D.A., Slovak, M.L., and Forman, S.J. (2003). Persistence of malignant hematopoietic progenitors in chronic myelogenous leukemia patients in complete cytogenetic remission following imatinib mesylate treatment. Blood *101*, 4701–4707.

Bohlson, S.S., Silva, R., Fonseca, M.I., and Tenner, A.J. (2005a). CD93 is rapidly shed from the surface of human myeloid cells and the soluble form is detected in human plasma. J. Immunol. *175*, 1239–1247.

Bohlson, S.S., Zhang, M., Ortiz, C.E., and Tenner, A.J. (2005b). CD93 interacts with the PDZ domain-containing adaptor protein GIPC: implications in the modulation of phagocytosis. J. Leukoc. Biol. *77*, 80–89.

Burman, J.L., Bourbonniere, L., Philie, J., Stroh, T., Dejgaard, S.Y., Presley, J.F., and McPherson, P.S. (2008). Scyl1, mutated in a recessive form of spinocerebellar neurodegeneration, regulates COPI-mediated retrograde traffic. J. Biol. Chem. *283*, 22774–22786.

Canitrot, Y., Laurent, G., Astarie-Dequeker, C., Bordier, C., Cazaux, C., and Hoffmann, J.S. (2006). Enhanced expression and activity of DNA polymerase β in chronic myelogenous leukemia. Anticancer Res. *26* (*1B*), 523–525.

Castelo-Branco, P., Zhang, C., Lipman, T., Fujitani, M., Hansford, L., Clarke, I., Harley, C.B., Tressler, R., Malkin, D., Walker, E., et al. (2011). Neural tumor-initiating cells have distinct telomere maintenance and can be safely targeted for telomerase inhibition. Clin. Cancer Res. *17*, 111–121.

Chen, T.R. (1985). Modal karyotype of human leukemia cell line, K562 (ATCC CCL 243). Cancer Genet. Cytogenet. *17*, 55–60.

Chevrier, S., Genton, C., Kallies, A., Karnowski, A., Otten, L.A., Malissen, B., Malissen, M., Botto, M., Corcoran, L.M., Nutt, S.L., and Acha-Orbea, H. (2009). CD93 is required for maintenance of antibody secretion and persistence of plasma cells in the bone marrow niche. Proc. Natl. Acad. Sci. USA *106*, 3895–3900.

Chu, S., McDonald, T., Lin, A., Chakraborty, S., Huang, Q., Snyder, D.S., and Bhatia, R. (2011). Persistence of leukemia stem cells in chronic myelogenous

leukemia patients in prolonged remission with imatinib treatment. Blood *118*, 5565–5572.

Cokol, M., Nair, R., and Rost, B. (2000). Finding nuclear localization signals. EMBO Rep. *1*, 411–415.

Dean, Y.D., McGreal, E.P., Akatsu, H., and Gasque, P. (2000). Molecular and cellular properties of the rat AA4 antigen, a C-type lectin-like receptor with structural homology to thrombomodulin. J. Biol. Chem. *275*, 34382–34392.

Dean, Y.D., McGreal, E.P., and Gasque, P. (2001). Endothelial cells, megakaryoblasts, platelets and alveolar epithelial cells express abundant levels of the mouse AA4 antigen, a C-type lectin-like receptor involved in homing activities and innate immune host defense. Eur. J. Immunol. *31*, 1370–1381.

Deville, L., Hillion, J., and Ségal-Bendirdjian, E. (2009). Telomerase regulation in hematological cancers: a matter of stemness? Biochim. Biophys. Acta *1792*, 229–239.

Dull, T., Zufferey, R., Kelly, M., Mandel, R.J., Nguyen, M., Trono, D., and Naldini, L. (1998). A third-generation lentivirus vector with a conditional packaging system. J. Virol. *72*, 8463–8471.

Gerber, J.M., Gucwa, J.L., Esopi, D., Gurel, M., Haffner, M.C., Vala, M., Nelson, W.G., Jones, R.J., and Yegnasubramanian, S. (2013). Genome-wide comparison of the transcriptomes of highly enriched normal and chronic myeloid leukemia stem and progenitor cell populations. Oncotarget *4*, 715–728.

Gorer, P.A. (1950). Studies in antibody response of mice to tumour inoculation. Br. J. Cancer *4*, 372–379.

Greenlee, M.C., Sullivan, S.A., and Bohlson, S.S. (2008). CD93 and related family members: their role in innate immunity. Curr. Drug Targets *9*, 130–138.

Greenlee, M.C., Sullivan, S.A., and Bohlson, S.S. (2009). Detection and characterization of soluble CD93 released during inflammation. Inflamm. Res. *58*, 909–919.

Herrmann, H., Sadovnik, I., Eisenwort, G., Rülicke, T., Blatt, K., Herndlhofer, S., Willmann, M., Stefanzl, G., Baumgartner, S., Greiner, G., et al. (2020). Delineation of target expression profiles in CD34+/CD38- and CD34+/CD38+ stem and progenitor cells in AML and CML. Blood Adv. *4*, 5118–5132.

Holst, J., Szymczak-Workman, A.L., Vignali, K.M., Burton, A.R., Workman, C.J., and Vignali, D.A.A. (2006). Generation of T-cell receptor retrogenic mice. Nat. Protoc. *1*, 406–417.

Holyoake, T.L., and Vetrie, D. (2017). The chronic myeloid leukemia stem cell: stemming the tide of persistence. Blood *129*, 1595–1606.

Horne, G.A., and Copland, M. (2017). Approaches for targeting self-renewal pathways in cancer stem cells: implications for hematological treatments. Expert Opin. Drug Discov. *12*, 465–474.

Hu, Y., and Smyth, G.K. (2009). ELDA: extreme limiting dilution analysis for comparing depleted and enriched populations in stem cell and other assays. J. Immunol. Methods *347*, 70–78.

Huang, H., and Auerbach, R. (1993). Identification and characterization of hematopoietic stem cells from the yolk sac of the early mouse embryo. Proc. Natl. Acad. Sci. USA *90*, 10110–10114.

Huntly, B.J., and Gilliland, D.G. (2005). Leukaemia stem cells and the evolution of cancer-stem-cell research. Nat. Rev. Cancer *5*, 311–321.

Iwasaki, M., Liedtke, M., Gentles, A.J., and Cleary, M.L. (2015). CD93 marks a non-quiescent human leukemia stem cell population and is required for development of MLL-rearranged acute myeloid leukemia. Cell Stem Cell *17*, 412–421.

Jabbour, E.J., Cortes, J.E., and Kantarjian, H.M. (2013). Tyrosine kinase inhibition: a therapeutic target for the management of chronic-phase chronic myeloid leukemia. Expert Rev. Anticancer Ther. *13*, 1433–1452.

Kanamoto, N., Akamizu, T., Tagami, T., Hataya, Y., Moriyama, K., Takaya, K., Hosoda, H., Kojima, M., Kangawa, K., and Nakao, K. (2004). Genomic structure and characterization of the 5′-flanking region of the human ghrelin gene. Endocrinology *145*, 4144–4153.

Kato, M., Yano, K., Morotomi-Yano, K., Saito, H., and Miki, Y. (2002). Identification and characterization of the human protein kinase-like gene NTKL: mitosis-specific centrosomal localization of an alternatively spliced isoform. Genomics *79*, 760–767.

Khan, K.A., Naylor, A.J., Khan, A., Noy, P.J., Mambretti, M., Lodhia, P., Athwal, J., Korzystka, A., Buckley, C.D., Willcox, B.E., et al. (2017). Multimerin-2 is a ligand for group 14 family C-type lectins CLEC14A, CD93 and CD248 spanning the endothelial pericyte interface. Oncogene *36*, 6097–6108.

Kinstrie, R., Horne, G.A., Morrison, H., Irvine, D., Munje, C., Castañeda, E.G., Moka, H.A., Dunn, K., Cassels, J.E., Parry, N., et al. (2020). CD93 is expressed on chronic myeloid leukemia stem cells and identifies a quiescent population which persists after tyrosine kinase inhibitor therapy. Leukemia.

Lago, S.G., Tomasik, J., van Rees, G.F., Steeb, H., Cox, D.A., Rustogi, N., Ramsey, J.M., Bishop, J.A., Petryshen, T., Haggarty, S.J., et al. (2019). Drug discovery for psychiatric disorders using high-content single-cell screening of signaling network responses ex vivo. Sci. Adv. *5*, eaau9093.

Laneuville, P. (2017). Stopping second-generation TKIs in CML. Blood *129*, 805–806.

Lapidot, T., Sirard, C., Vormoor, J., Murdoch, B., Hoang, T., Caceres-Cortes, J., Minden, M., Paterson, B., Caligiuri, M.A., and Dick, J.E. (1994). A cell initiating human acute myeloid leukaemia after transplantation into SCID mice. Nature *367*, 645–648.

Liu, S.C.H., Lane, W.S., and Lienhard, G.E. (2000). Cloning and preliminary characterization of a 105 kDa protein with an N-terminal kinase-like domain. Biochim. Biophys. Acta *1517*, 148–152.

Lorenzon, E., Colladel, R., Andreuzzi, E., Marastoni, S., Todaro, F., Schiappacassi, M., Ligresti, G., Colombatti, A., and Mongiat, M. (2012). MULTIMERIN2 impairs tumor angiogenesis and growth by interfering with VEGF-A/VEGFR2 pathway. Oncogene *31*, 3136–3147.

Løvik, G., Vaage, J.T., Dissen, E., Szpirer, C., Ryan, J.C., and Rolstad, B. (2000). Characterization and molecular cloning of rat C1qRp, a receptor on NK cells. Eur. J. Immunol. *30*, 3355–3362.

Ma, X., Husain, T., Peng, H., Lin, S., Mironenko, O., Maun, N., Johnson, S., Tuck, D., Berliner, N., Krause, D.S., and Perkins, A.S. (2002). Development of a murine hematopoietic progenitor complementary DNA microarray using a subtracted complementary DNA library. Blood *100*, 833–844.

Magueur, E., Hagege, H., Attali, P., Singlas, E., Etienne, J.P., and Taburet, A.M. (1991). Pharmacokinetics of metoclopramide in patients with liver cirrhosis. Br. J. Clin. Pharmacol. *31*, 185–187.

Marian, C.O., Cho, S.K., McEllin, B.M., Maher, E.A., Hatanpaa, K.J., Madden, C.J., Mickey, B.E., Wright, W.E., Shay, J.W., and Bachoo, R.M. (2010a). The telomerase antagonist, imetelstat, efficiently targets glioblastoma tumor-initiating cells leading to decreased proliferation and tumor growth. Clin. Cancer Res. *16*, 154–163.

Marian, C.O., Wright, W.E., and Shay, J.W. (2010b). The effects of telomerase inhibition on prostate tumor-initiating cells. Int. J. Cancer *127*, 321–331.

McGreal, E., and Gasque, P. (2002). Structure-function studies of the receptors for complement C1q. Biochem. Soc. Trans. *30*, 1010–1014.

McGreal, E.P., Ikewaki, N., Akatsu, H., Morgan, B.P., and Gasque, P. (2002). Human C1qRp is identical with CD93 and the mNI-11 antigen but does not bind C1q. J. Immunol. *168*, 5222–5232.

McKearn, J.P., McCubrey, J., and Fagg, B. (1985). Enrichment of hematopoietic precursor cells and cloning of multipotential B-lymphocyte precursors. Proc. Natl. Acad. Sci. USA *82*, 7414–7418.

Medina, M., and Dotti, C.G. (2003). RIPped out by presenilin-dependent γ-secretase. Cell. Signal. *15*, 829–841.

Neering, S.J., Bushnell, T., Sozer, S., Ashton, J., Rossi, R.M., Wang, P.Y., Bell, D.R., Heinrich, D., Bottaro, A., and Jordan, C.T. (2007). Leukemia stem cells in a genetically defined murine model of blast-crisis CML. Blood *110*, 2578–2585.

Nepomuceno, R.R., Henschen-Edman, A.H., Burgess, W.H., and Tenner, A.J. (1997). cDNA cloning and primary structure analysis of C1qR(P), the human C1q/MBL/SPA receptor that mediates enhanced phagocytosis in vitro. Immunity *6*, 119–129.

Norsworthy, P.J., Fossati-Jimack, L., Cortes-Hernandez, J., Taylor, P.R., Bygrave, A.E., Thompson, R.D., Nourshargh, S., Walport, M.J., and Botto, M.

(2004). Murine CD93 (C1qRp) contributes to the removal of apoptotic cells in vivo but is not required for C1q-mediated enhancement of phagocytosis. J. Immunol. *172*, 3406–3414.

Ohyashiki, K., Ohyashiki, J.H., Iwama, H., Hayashi, S., Shay, J.W., and Toyama, K. (1997). Telomerase activity and cytogenetic changes in chronic myeloid leukemia with disease progression. Leukemia *11*, 190–194.

Okamoto, I., Kawano, Y., Matsumoto, M., Suga, M., Kaibuchi, K., Ando, M., and Saya, H. (1999). Regulated CD44 cleavage under the control of protein kinase C, calcium influx, and the Rho family of small G proteins. J. Biol. Chem. *274*, 25525–25534.

Okamoto, I., Kawano, Y., Murakami, D., Sasayama, T., Araki, N., Miki, T., Wong, A.J., and Saya, H. (2001). Proteolytic release of CD44 intracellular domain and its role in the CD44 signaling pathway. J. Cell Biol. *155*, 755–762.

Petrenko, O., Beavis, A., Klaine, M., Kittappa, R., Godin, I., and Lemischka, I.R. (1999). The molecular characterization of the fetal stem cell marker AA4. Immunity *10*, 691–700.

Radich, J.P., Dai, H., Mao, M., Oehler, V., Schelter, J., Druker, B., Sawyers, C., Shah, N., Stock, W., Willman, C.L., et al. (2006). Gene expression changes associated with progression and response in chronic myeloid leukemia. Proc. Natl. Acad. Sci. USA *103*, 2794–2799.

Ramalho-Santos, M. (2002). "Stemness": transcriptional profiling of embryonic and adult stem cells. Science *298*, 597–600.

Riether, C., Schürch, C.M., and Ochsenbein, A.F. (2015a). Regulation of hematopoietic and leukemic stem cells by the immune system. Cell Death Differ. *22*, 187–198.

Riether, C., Gschwend, T., Huguenin, A.L., Schürch, C.M., and Ochsenbein, A.F. (2015b). Blocking programmed cell death 1 in combination with adoptive cytotoxic T-cell transfer eradicates chronic myelogenous leukemia stem cells. Leukemia *29*, 1781–1785.

Riether, C., Schürch, C.M., Flury, C., Hinterbrandner, M., Drück, L., Huguenin, A.L., Baerlocher, G.M., Radpour, R., and Ochsenbein, A.F. (2015c). Tyrosine kinase inhibitor-induced CD70 expression mediates drug resistance in leukemia stem cells by activating Wnt signaling. Sci. Transl. Med. *7*, 298ra119.

Saito, Y., Kitamura, H., Hijikata, A., Tomizawa-Murasawa, M., Tanaka, S., Takagi, S., Uchida, N., Suzuki, N., Sone, A., Najima, Y., et al. (2010). Identification of therapeutic targets for quiescent, chemotherapy-resistant human leukemia stem cells. Sci. Transl. Med. *2*, 17ra9.

Savona, M., and Talpaz, M. (2008). Getting to the stem of chronic myeloid leukaemia. Nat. Rev. Cancer *8*, 341–350.

Schroeter, E.H., Kisslinger, J.A., and Kopan, R. (1998). Notch-1 signalling requires ligand-induced proteolytic release of intracellular domain. Nature *393*, 382–386.

Schürch, C.M., Riether, C., and Ochsenbein, A.F. (2014). Cytotoxic CD8+ T cells stimulate hematopoietic progenitors by promoting cytokine release from bone marrow mesenchymal stromal cells. Cell Stem Cell *14*, 460–472.

Shalaby, M.A.F., Latif, H.A., and Sayed, M.E. (2013). Interaction of insulin with prokinetic drugs in STZ-induced diabetic mice. World J. Gastrointest. Pharmacol. Ther. *4*, 28–38.

Shay, J.W., and Wright, W.E. (2010). Telomeres and telomerase in normal and cancer stem cells. FEBS Lett. *584*, 3819–3825.

Sjöqvist, M., Antfolk, D., Ferraris, S., Rraklli, V., Haga, C., Antila, C., Mutvei, A., Imanishi, S.Y., Holmberg, J., Jin, S., et al. (2014). PKCζ regulates Notch receptor routing and activity in a Notch signaling-dependent manner. Cell Res. *24*, 433–450.

Soltis, R.D., Hasz, D., Morris, M.J., and Wilson, I.D. (1979). The effect of heat inactivation of serum on aggregation of immunoglobulins. Immunology *36*, 37–45.

Stewart, S.A., Dykxhoorn, D.M., Palliser, D., Mizuno, H., Yu, E.Y., An, D.S., Sabatini, D.M., Chen, I.S., Hahn, W.C., Sharp, P.A., Weinberg, R.A., and Novina, C.D. (2003). Lentivirus-delivered stable gene silencing by RNAi in primary cells. RNA *9*, 493–501.

Tatematsu, K., Nakayama, J., Danbara, M., Shionoya, S., Sato, H., Omine, M., and Ishikawa, F. (1996). A novel quantitative 'stretch PCR assay', that detects a dramatic increase in telomerase activity during the progression of myeloid leukemias. Oncogene *13*, 2265–2274.

Verstovsek, S., Kantarjian, H., Manshouri, T., Cortes, J., Faderl, S., Giles, F.J., Keating, M., and Albitar, M. (2003). Increased telomerase activity is associated with shorter survival in patients with chronic phase chronic myeloid leukemia. Cancer *97*, 1248–1252.

Warde-Farley, D., Donaldson, S.L., Comes, O., Zuberi, K., Badrawi, R., Chao, P., Franz, M., Grouios, C., Kazi, F., Lopes, C.T., et al. (2010). The GeneMANIA prediction server: biological network integration for gene prioritization and predicting gene function. Nucleic Acids Res. *38*, W214-20.

Wick, M., Zubov, D., and Hagen, G. (1999). Genomic organization and promoter characterization of the gene encoding the human telomerase reverse transcriptase (hTERT). Gene *232*, 97–106.

Zhang, M., Bohlson, S.S., Dy, M., and Tenner, A.J. (2005). Modulated interaction of the ERM protein, moesin, with CD93. Immunology *115*, 63–73.

Zhao, Y., Zheng, J., Ling, Y., Hou, L., and Zhang, B. (2005). Transcriptional upregulation of DNA polymerase β by TEIF. Biochem. Biophys. Res. Commun. *333*, 908–916.

STAR★METHODS

KEY RESOURCES TABLE

REAGENT or RESOURCE	SOURCE	IDENTIFIER
Antibodies		
Anti-mouse c-kit-PE-Cy7	BioLegend	Cat# 105813, RRID:AB_313222
Anti-mouse c-kit-APC-Cy7	BioLegend	Cat# 105826, RRID:AB_1626278
Anti-mouse Sca-1-PerCP-Cy5.5	BioLegend	Cat# 1 08123, RRID:AB_893619
Anti-mouse CD16/32-PE-Cy7	BioLegend	Cat# 101318, RRID:AB_2104156
Anti-mouse CD90.2-Alexa Fluor 700	BioLegend	Cat# 105320, RRID:AB_493725
Anti-mouse CD150-Pacific Blue	BioLegend	Cat# 115923, RRID:AB_2187962
Anti-mouse CD127-PE	BioLegend	Cat# 121111, RRID:AB_493510
Anti-mouse CD48-Alexa Fluor 700	BioLegend	Cat# 103425, RRID:AB_10612754
Anti-mouse GR1-PE	BioLegend	108407, RRID:AB_313372
Anti-mouse GR1-biotin	BioLegend	Cat# 108404, RRID:AB_313369
Anti-mouse CD135-PE	BioLegend	135306, RRID:AB_1877217
Anti-mouse CD19-APC-Cy7	BioLegend	Cat# 115530, RRID:AB_830707
Anti-mouse CD19-biotin	BioLegend	Cat# 115503, RRID:AB_313638
Anti-mouse CD11b-PE-Cy7	BioLegend	Cat# 101216, RRID:AB_312799
Anti-mouse CD3ε-biotin	BioLegend	Cat# 100304, RRID:AB_312669
Anti-mouse Ter119-biotin	BioLegend	Cat# 116203, RRID:AB_313704
Anti-mouse CD93-APC	BioLegend	Cat# 136509, RRID:AB_2275879
Rat IgG2b, k APC	BioLegend	Cat# 400611, RRID:AB_326555
Anti-mouse CD34-eFluor 450	Thermo Fisher Scientific	Cat# 48-0341-82, RRID:AB_2043837
Anti-human CD34-APC	BioLegend	Cat# 343608, RRID:AB_2228972
Anti-human CD34-APC-Cy7	BioLegend	Cat# 343513, RRID:AB_1877169
Anti-human CD45-Pacific Blue	BioLegend	Cat# 304022, RRID:AB_493655
Anti-human CD38-PE-Cy7	BioLegend	303515, RRID:AB_1279235
Anti-human CD2-biotin	Biolegend	Cat# 300204, RRID:AB_314028
Anti-human CD90-PerCP-Cy5.5	BioLegend	Cat# 328118, RRID:AB_2303335
Anti-human CD3-biotin	Biolegend	Cat# 317320, RRID:AB_10916519
Anti-human CD14-biotin	BioLegend	Cat# 325624, RRID:AB_2074052
Anti-human CD16-biotin	BioLegend	Cat# 302004, RRID:AB_314204
Anti-human CD19-biotin	BioLegend	Cat# 302203, RRID:AB_314233
Anti-human CD56-biotin	BioLegend	Cat# 318320, RRID:AB_893390
Anti-human CD235ab-biotin	BioLegend	Cat# 306618, RRID:AB_2565773
Anti-human CD93	Sigma	HPA009300, RRID:AB_1846342
Anti-Rabbit IgG (H+L) Alexa Fluor Plus 647	Thermo Fisher Scientific	Cat# A32733, RRID:AB_2633282
Anti-GFP antibody	Abcam	Cat# ab290, RRID:AB_303395
Anti-Lamin B1 antibody	Abcam	Cat# ab16048, RRID:AB_443298
Alpha Tubulin antibody	Abcam	Cat# ab7291, RRID:AB_2241126
Anti-mouse IgG, HRP-linked Antibody	Cell Signaling	Cat# 7076, RRID:AB_330924
Anti-rabbit IgG, HRP-linked Antibody	Cell Signaling	Cat# 7074, RRID:AB_2099233
Anti-human CD34	Cell Marque	Cat# 134M-16, RRID:AB_1159227
Anti-human CD93	Abcam	Cat# ab134079. RRID:n.k.
Anti-rabbit IgG (H+L), F(ab')2 Fragment Alexa Fluor 488	Cell Signaling	Cat# 4412, RRID:AB_1904025

(*Continued on next page*)

Continued

REAGENT or RESOURCE	SOURCE	IDENTIFIER
Bacterial and virus strains		
Platinum-E (Plat-E)	Cell Biolabs	Cat# RV-10
293FT	Thermo Fisher Scientific	Cat# R7007
Biological samples		
BM aspirates from untreated, newly diagnosed CML patients	Department of Hematology and Central Hematology Laboratory, Inselspital, Bern University Hospital and University of Bern	N/A
BM from healthy donors (orthopedic patients who underwent Vertebroplasty)	Inselspital, Bern University Hospital and University of Bern	N/A
Chemicals, peptides, and recombinant proteins		
Methylcellulose	STEMCELL Technologies	Cat# 03134
Screen-Well® FDA Approved Drug Library V2 version 1.2	Enzo	Cat# BML-2843-0100
Metoclopramide	Sigma	Cat# M0763. CAS: 7232-21-5 (hydrochloride)
Lipofectamine LTX	Thermo Fisher Scientific	Cat# 115338500
Polybrene	Sigma	Cat# H9268. CAS: 28728-55-4
Puromycin	Sigma	Cat# P8833. CAS: 58-58-2 (dihydrochloride)
Nilotinib	Novartis	Sigma
PKC 20-28	Merck Millipore	Cat# 476480
Streptavidin-BD Horizon V500	BD PharMingen	Cat# 561419, RRID:AB_10611863
Fixable viability dye-eFluor450	Thermo Fisher Scientific	Cat# 65-0863-14
Fixable viability dye-eFluor780	Thermo Fisher Scientific	Cat# 65-0865-14
DAKO Wash	DAKO	Cat# S300685-2
DAKO diluent	DAKO	Cat# S0809
DAPI	Thermo Fisher Scientific	Cat# D1306
NucRed Live 647 ReadyProbes	Thermo Fisher Scientific	Cat# R37106
EcoRI	New England BioLabs	Cat# R0101M
XhoI	New England BioLabs	Cat# R0146M
NP40	Thermo Fisher Scientific	Cat# 28324
Laemmli buffer	Biorad	Cat# 610747
Mini-PROTEAN® TGX Stain-Free Protein Gels	Biorad	Cat# 4568096
Trans-Blot® Turbo RTA Mini PVDF Transfer Kit	Biorad	Cat# 1704272
Clarity Western ECL Substrate	Biorad	Cat# 1705060
Aquatex	Merck Millipore	Cat# 108562
BrDU	Sigma	Cat# B5002. CAS Number 59-14-3
Critical commercial assays		
DAB Detection kit	Leica Biosystems	Cat# DS9800
SuperScript III Reverse Transcriptase kit	Thermo Fisher Scientific	Cat# 18080085
Bond Polymer Refine Red Detection kit	Leica Biosystems	Cat# DS9390
TruSeq ChIP Sample Prep Kit	Illumina	IP-202-1012
RNA Easy Micro Kit	QIAGEN	Cat# 74004
Quantifluor RNA System Kit	Promega	Cat# E3310
SMART-Seq v4 Ultra Low Input RNA Kit	Takara Bio	Cat# 634894
High Sensitivity NGS Fragment Analysis Kit	Agilent	Cat# DNF-474-0500
BD PharMingen BrdU Flow Kit	BD PharMingen	Cat# 552598

(*Continued on next page*)

Continued

REAGENT or RESOURCE	SOURCE	IDENTIFIER
Deposited data		
Raw and analyzed data	This paper	GEO: GSE149358
Primer sequences	This paper	Tables S4 and S6
Experimental models: cell lines		
K562	ATCC	ATCC CCL-243. RRID:CVCL_0004
EL4	ATCC	ATCC TIB-39. RRID:CVCL_0255
STR-4	Aizawa et al., 1991	N/A
Experimental models: organisms/strains		
Mouse: C57BL/6J	Charles River	Strain Code 632
Mouse: CD93$^{-/-}$	Norsworthy et al., 2004	N/A
Oligonucleotides		
siRNA targeting human CD93	Santa Cruz Biotechnolgy	Cat#: sc-105157
esiRNA targeting murine Scyl1	Sigma	Cat#: EMU022211
shRNA targeting murine CD93	Santa Cruz Biotechnolgy	Cat#: sc-106980-V
Control scrambled shRNA lentiviral particles	Santa Cruz Biotechnolgy	Cat#: sc-108080
Actb, FW: AGATGACCCAGATCAT GTTTGAG	This paper	N/A
Actb, RV: GTACGACCAGAGGCATACAG	This paper	N/A
Ccnd2, FW: TGGATGCTAGAGGTC TGTGAG	This paper	N/A
CCnd2, RV: GGATGGTCTCTTTCAG CTTGG	This paper	N/A
Cd93, FW: CAGTACAGCCCAACACCAG	This paper	N/A
Cd93, RV: GAGAGTCCAGTCAAGTCA TTCAG	This paper	N/A
Cdk4, FW: AATGTTGTACGGCTGATGG	This paper	N/A
Cdk4, RV: GTGCTTTGTCCAGGTATGTC	This paper	N/A
Gapdh, FW: AGAACATCATCCCTGCATCC	This paper	N/A
Gapdh, FW: TCATCATACTTGGCAGGT TTCTC	This paper	N/A
Additional primer sequences for qRT-PCR	This paper	Table S4
Recombinant DNA		
pLVX-AcGFP1-N1	Clontech	Cat#: 632154
pMSCV-IRES-GFP II	Addgene, Holst et al., 2006	Cat#: 52107
pMSCV-IRES-CFP II	Addgene, Holst et al., 2006	Cat#: 52109
pMDLg/pRRE	Addgene, Dull et al., 1998	Cat#: 12251
pRSV-Rev	Addgene, Dull et al., 1998	Cat#: 12253
pCMV-VSV-G	Addgene, (Stewart et al., 2003)	Cat#: 8454
pLVX-AcGFP1-N1-Cd93	This paper	N/A
pMSCV-IRES-GFP-Cd93	This paper	N/A
pMSCV-IRES-GFP-Scyl1	This paper	N/A
pMSCV-IRES-GFP-BCR-ABL1	This paper, Riether et al., 2015b	N/A
pMSCV-IRES-CFP-BCR-ABL1	This paper	N/A
SCYL1 Gene ORF cDNA clone	Sino Biological	Cat#: MG51756-NM
Software and algorithms		
FlowJo software v.10.6	TreeStar	N/A
Phobius database	Stockholm Bioinformatics Center	https://phobius.sbc.su.se/
IDEAS image analysis software	Merck Millipore	N/A

(*Continued on next page*)

Continued

REAGENT or RESOURCE	SOURCE	IDENTIFIER
Illumina RTA version 2.4.11	Illumina	N/A
bcl2fastq v2.20.0.422.	Illumina	N/A
SeqMan NGen software v.15	DNASTAR	N/A
ArrayStar software v.15	DNASTAR	N/A
Partek® Genomics SuiteTM software, v.7	Partek	N/A
GSEA software v.3.0	Broad Institute	https://software.broadinstitute.org/cancer/software/gsea/wiki/index.php/GSEA_v3.0_Release_Notes
Pathcards database	Weizmann Institute of Science	https://pathcards.genecards.org/
RAMALHO_STEMNESS_UP	Ramalho-Santos, 2002	https://www.gsea-msigdb.org/gsea/msigdb/cards/RAMALHO_STEMNESS_UP
MA_MYELOID_DIFFERENTIATION_UP	Ma et al., 2002	https://www.gsea-msigdb.org/gsea/msigdb/cards/MA_MYELOID_DIFFERENTIATION_UP
ELDA software	Hu and Smyth, 2009	http://bioinf.wehi.edu.au/software/elda/)
GraphPad Prism® software v7.0	GraphPad	N/A

RESOURCE AVAILABILITY

Lead contact

Further information and requests for resources and reagents should be directed to and will be fulfilled by the lead contact, Carsten Riether (carsten.riether@dbmr.unibe.ch).

Materials availability

All unique reagent generated in this study are available from the Lead Contact without restriction.

Data and code availability

All RNA-seq data compiled for this study is made publicly available on the Gene Expression Omnibus (GEO) website (https://www.ncbi.nlm.nih.gov/geo/) under the accession number GSE149358. This study does not include the development of new code.

EXPERIMENTAL MODEL AND SUBJECT DETAILS

Patient samples

BM aspirates from untreated, newly diagnosed CML patients at the Department of Hematology and Central Hematology Laboratory, Inselspital, Bern University Hospital and University of Bern, Switzerland, were obtained after written informed consent. BM from healthy donors was collected from orthopedic patients who underwent Vertebroplasty. Patient characteristics are listed in Table S3. Analysis of BM samples was approved by the local ethical committee of the Canton of Bern, Switzerland (KEK 122/14 and 2019-01627).

Cell lines

The leukemia cell line BCR-ABL1-expressing leukemia cell lines K562 (Chen, 1985) and EL-4 (Gorer, 1950) were purchased from ATCC, the Platinum-E (Plat-E) Packaging Cell Line from Cell Biolabs (cat. RV-10) and the 293FT packaging cell line from ThermoFisher (cat. R70007). Therefore, no additional authentication was performed. The BM endothelial cell line STR-4 (Aizawa et al., 1991) was kindly provided by Prof. M. Manz (University Hospital Zürich, Switzerland). The cells line were tested mycoplasma-free and was were grown in FCS-containing medium recommended by ATCC (http://www.atcc.org/?geo_country=us) or by Cell Biolabs and ThermoFisher supplemented with 100U/ml penicillin, and 100 μg/ml of streptomycin in a humidified atmosphere of 95% air and 5% CO_2 at 37°C at a low passage number. Media were routinely changed every 3 days (Chen, 1985).

Mice

C57BL/6J (BL/6) mice were from Charles Rivers (Sulzfeld, Germany). *Cd93*$^{-/-}$ on BL/6 background were provided by Prof. Hans Acha-Orbea (University of Lausanne). BL/6 background was confirmed by SNP analysis performed at Taconic. Experiments were performed with age- (6-8 weeks) and sex-matched animals of both genders. Mice were housed under specific pathogen–free

conditions in individually ventilated cages with food and water *ad libitum* and were regularly monitored for pathogens. Animal experiments were approved by the local experimental animal committee of the Canton of Bern and performed according to Swiss laws for animal protection.

METHOD DETAILS

Study design

In hypothesis-driven experimental designs, we addressed the molecular mechanisms of *Cd93*-signaling in LSCs in a murine model of CML using BL/6 and *Cd93*$^{-/-}$ mice and how *Cd93*-signaling can be pharmacologically targeted. In addition, leukemia development, survival, LSC proliferation and LSC functionality was assessed. All experiments were performed with 6- to 8-week-old mice housed in a specific pathogen-free facility in individually ventilated cages. Food was provided *ad libitum*. Mice were assigned randomly to different treatment groups. These investigations were extended to CML cell lines and primary BM and leukapheresis samples from newly diagnosed CML patients to further investigate the molecular mechanisms and demonstrate the human relevance of the findings.

All experiments were conducted and analyzed in a non-blinded fashion. Information on biological and technical replicates are indicated in figure legends.

Antibodies

Mouse: αc-kit-PE-Cy7 (cat. 105813, clone 2B8, 1:600), and -APC-Cy7 (cat. 105826, clone 2B8, 1:300), αSca-1-PerCP-Cy5.5 (cat. 108123, clone D7, 1:600), αCD16/32-PE-Cy7 (cat. 101318, clone 93, 1:200), αCD90.2-AlexaFluor 700 (cat. 105320, clone 30-H12, 1:100), αCD150-Pacific Blue (cat. 115923, clone TC15-12.2, 1:100), αCD127-PE (cat. 121111, clone SB/199, 1:100), αCD48-AlexaFluor 700 (cat. 103425, clone HM48-1, 1:100), αGr-1-PE (cat. 108407, clone: RB6-8C5, 1:400), αGr-1-biotin (cat. 108404, clone RB6-8C5, 1:300), αCD135-PE (cat. 135306, clone A2F10, 1:100), αCD19-APC-Cy7 (cat. 115530, clone 6D5, 1:300) and CD19-biotin (cat. 115503, clone 6D5, 1:300), αCD11b-PE-Cy7 (cat. 101216, clone M1/70, 1:200), αCD3ε-biotin (cat. 100304, clone 145-2C11, 1:300), αTer119-biotin (cat. 116203, clone Ter-119, 1:300), αCD93-APC (cat. 136509, clone AA4.1, 1:200) and the corresponding isotype control (cat. 400611, clone RTK4530) were from BioLegend. αCD34-eFluor 450 (cat. 48-0341-82, clone RAM34, 1:100) was from Thermo Fisher. Streptavidin-BD Horizon V500 was from BD PharMingen (cat. 561419, 1:1000). Lineage depletion was performed with a cocktail of lineage-specific antibodies (αCD3α-biotin, αCD19-biotin, αGr-1-biotin, αTer119-biotin, listed above in detail) using αbiotin microbeads and autoMACS system (Miltenyi Biotec).

Human: αCD34-APC (cat. 343608, clone 561, 1:80) and αCD34-APC-Cy7 (cat. 343513, clone 561, 1:100), αCD45-Pacific-Blue (cat. 304022, clone HI30, 1:300), αCD38-PE-Cy7 (cat. 303515, clone HIT2, 1:50) and αCD90-PerCP-Cy5.5 (cat. 328118, clone 5E10, 1:100) were from BioLegend. Lineage-positive cells were excluded by staining using biotinylated αCD2 (cat. 300204, clone RPA2.10, 1:100), αCD3 (cat. 317320, clone OKT3, 1:100), αCD14 (cat. 325624, clone HCD14, 1:100), αCD16 (cat. 302004, clone 3G8, 1:100), αCD19 (cat. 302203, clone HIB19, 1:100), αCD56 (cat. 318320, clone HCD56, 1:100) and αCD235ab (cat. 306618, clone HIR2, 1:100) (BioLegend), followed by a second step using streptavidin-BD-Horizon-V500 (cat. 561419, 1:1000, BD PharMingen). αCD93 (cat. HPA009300, 1:50) was from Sigma. αCD93 (cat. ab134079, 1:1000) was from Abcam. Anti-rabbit IgG (H+L), F(ab')2 Fragment Alex Fluor 488 was from Cell signaling (cat. 4412, 1:1000). Goat-anti-rabbit Alexa647 secondary antibody was from Thermo Fisher Scientific (cat. A32733, 1:2000). Fixable viability dye-eFluor450 (cat. 65-0863-14, 1:4000) and eFluor780 (cat. 65-0865-14, 1:5000) was from Thermo Fisher Scientific

Samples were acquired on a BD LSRFortessa and sorting procedures were conducted using a BD FACS Aria III (BD Biosciences). Data were analyzed using FlowJo software v.10.6 (TreeStar).

All primary antibodies for Western Blot were purchased from Abcam: αGFP (cat. ab290, 1:1000), α-lamin B1 (cat. Ab16048, 1:1000), α-alpha tubulin (DM1A) (cat. ab7291, 1:1000). All secondary antibodies were purchased from Cell signaling: α-mouse IgG (cat. 7076, 1:10000), α−rabbit IgG (cat. 7074, 1:10000).

Colony assays

Colony assays from BM lin$^-$ cells of CML and naive mice and CD34$^+$ stem/progenitor cells of human CML patients were performed as described before (Riether et al., 2015c).

For mouse colony assays 10^3 FACS-purified LSKs or LSCs were plated in methylcellulose (cat. 03134, STEMCELL Technologies) and colonies were enumerated 7 days later. For serial re-plating experiments, 10^4 cells were collected from preceding colony assays and replated in methylcellulose. Colonies were enumerated after seven days.

For the drug library screen, we used compounds from the Screen-Well® FDA Approved Drug Library V2 version 1.2 (cat. BML-2843-0100, Enzo, Table S2). For this assay, 10^3 FACS-purified murine LSCs were incubated overnight in 96 well V-bottom plates in the presence of 1 μM compound (Table S2) or vehicle followed by plating methylcellulose. Colonies were enumerated after seven days.

For experiments using metoclopramide (cat. M0763, Sigma), 10^3 FACS-purified murine LSCs or $2x10^3$ human CD34$^+$ stem/progenitor cells were incubated overnight in 96 well V-bottom plates in the presence of 0.1 and 1 μM metoclopramide, 5 μM nilotinib or vehicle followed by plating methylcellulose. Colonies were enumerated 7 days and 14 days later, respectively.

For re-plating assays 10^4 or $2x10^4$ cells isolated from primary mouse and human colony assays, respectively, were subsequently replated in methylcellulose in the absence of any compound. Colony were enumerated 7 days and 14 days later.

Gene silencing of CD93, Cd93 and Scyl1

siRNA: Human *CD93* and murine *Scyl1* genes were silenced in human $lin^-CD90^+CD34^+$ BM cells and murine LSCs respectively using siRNA and esiRNA according to the manufacturer's instructions (Santa Cruz Biotechnology (cat. sc-105157) and Sigma (cat. EMU022211), respectively) with minor modifications to increase silencing efficiency. Briefly, siRNA, esiRNA or scrambled controls were mixed with transfection medium and Lipofectamine LTX (cat. 15338500, Thermo Fisher Scientific) in serum-free transfection media. Cells were subsequently treated with transfection complexes in the presence of antibiotic-free growth medium overnight and were further used for functional assays and determination of the expression for selected genes of interest.

shRNA: *Cd93* mRNA was silenced in murine LSCs using ready-to-use lentiviral particles (sh*Cd93*: cat. sc-106980-V; scr: cat. sc-108080, Santa Cruz Biotechnology). Briefly, $5x10^4$ LSCs cells were transduced overnight by spin-transfection at 37°C and 5% CO_2 with virus of sh*Cd93* lentiviral particles or the respective control scrambled RNA lentiviral particles (MOI: 5, Santa Cruz Biotechnology Inc.) in the presence of 5 μg/ml polybrene (cat. H9268, Sigma). After spin transfection, medium was removed, and cells were cultured in medium supplemented with 1 μg/ml puromycin (cat. P8833, Sigma) for 48h to select for stable expression of sh*Cd93* or scrambled (scr) RNA.

Overexpression of mCd93

The mouse *Cd93* gene (ENSMUSG00000027435; *mCd93*) was cloned from FACS-purified B cell precursors. cDNA synthesis was carried out using SuperScript III Reverse Transcriptase kit (cat. 18080085, Thermo Fisher Scientific). The open reading frame (ORF) of *Cd93* with a total length of 1.932kb (644aa) was amplified by PCR using tagged primes for the restriction enzymes (EcoRI and XhoI, cat. R0101M and R0146M, New England BioLabs). In addition, the forward primer harbored the Kozak consensus sequence (GCCACC) before the start codon to enhance the protein translation. Next, the *Cd93* ORF was cloned into pMSCV-IRES-GFP II (pMIG II) plasmid (Holst et al., 2006)(cat. 52107, Addgene).

The $Cd93^{intra}$ construct, lacking the sequence encoding for the extracellular domain of *Cd93* was designed by cloning of the signal peptide (1-22aa), transmembrane (574-598aa) and cytoplasmic (599-644aa) domains of the *Cd93* ORF (total length of 282bp) into a pMIG II plasmid. To predict and select the different *Cd93* protein domains prior to cloning we used the Phobius database (https://phobius.sbc.su.se/).

Retroviral vectors expressing *Cd93* or $Cd93^{intra}$ were generated using Platinum-E (Plat-E) Packaging Cell Line (Cell Biolabs). Next, FACS-purified murine LSKs or CML LSCs derived from BL/6 and/or $Cd93^{-/-}$ mice were transduced with retroviral vectors expressing *Cd93*, $Cd93^{intra}$ or an empty vector as a control (mock). Two days after transduction, LSCs or LSKs expressing *Cd93*, $Cd93^{intra}$ or mock GFP were FACS-purified and plated in methylcellulose.

Overexpression of Scyl1

The mouse *Scyl1* gene (ENSMUSG00000024941; *mScyl1*) was sub-cloned from the SCYL1 Gene ORF cDNA clone (cat. MG51756-NM, Sino Biological). cDNA synthesis was carried out using SuperScript III Reverse Transcriptase kit (cat. 18080085, Thermo Fisher Scientific). The open reading frame (ORF) of *Scyl1* with a total length of 2.4kb (289aa) was amplified by PCR using tagged primes for the restriction enzymes (EcoRI and XhoI, cat. R0101M and R0146M, New England BioLabs). In addition, the forward primer harbored the Kozak consensus sequence (GCCACC) before the start codon to enhance the protein translation. Next, the *mScyl1* ORF was cloned into pMSCV-IRES-GFP II (pMIG II) plasmid (cat. 52107, Addgene).

Retroviral vectors expressing *Scyl1* were generated using Platinum-E (Plat-E) Packaging Cell Line (Cell Biolabs). Next, FACS-purified murine CML LSCs derived from BL/6 and/or $Cd93^{-/-}$ mice were transduced with retroviral vectors expressing *Scyl1* or an empty vector as a control (mock). Two days after transduction, LSCs expressing *Scyl1* or mock GFP were FACS-purified and plated in methylcellulose. Successful overexpression of *Scyl1* was assessed by qRT-PCR analysis.

Sub-cellular localization of mCd93

The mouse *Cd93* gene was cloned in pAcGFP1-N1 mammalian expressing plasmid and as the lentiviral construct pLVX-AcGFP1-N1 (cat. 632154, Clontech). Lentiviral particles (3rd generation) were generated into the 293FT packaging cell line (cat. R70007, Thermo Fisher Scientific) using pMDLg/pRRE, pRSV-Rev and pCMV-VSV-G plasmids (Dull et al., 1998)(Addgene). For transfection, adherent STR-4 cells were seeded at density 10^5 cells/well in antibiotics-free medium and left to adhere for 5h. Cells growing in suspension (K562 and EL4 cells) were seeded at a density 10^5 cells/well in antibiotics-free medium shortly before transfection. Liposomal transfection was performed with Lipofectamine LTX according to the manufacturers' instructions (cat. 15338500, Thermo Fisher Scientific), using the previously optimized conditions (per 10^5 cells: 0.25 μg plasmid DNA, 2.5 μL Lipofectamine LTX, and for K562 additionally 0.25 μL PLUS reagent). 48h post transfection/transduction, the expression of mCD93-GFP fusion protein was analyzed by ImageStream or Western Blot. For experiments with nilotinib, 70 μM of nilotinib or vehicle (DMSO) were added to the culture for 72h. For experiments using the PKC-α/β inhibitor PKC 20-28 (cat. 476480, Merck Millipore) or metoclopramide (cat. M0763, Sigma), 50 μM and 0.1 μM of compound or vehicle (H_20) were added to the culture for 72h, respectively.

ImageStream data acquisition and analysis

Briefly, cells expressing CD93-GFP were stained with fixable viability dye eFluor780 (cat. 65-0865-14, 1:5000, Thermo Fisher Scientific) for 30 min at 4°C. Cells were subsequently fixed with 4% paraformaldehyde for 10 min at room temperature and then permeabilized for 5 min at room temperature with DAKO Wash (cat. S300685-2, Dako) diluted in DAKO diluent (cat. S0809, Dako). After washing, nuclei were stained with 10 μg/ml DAPI (cat. D1306, Thermo Fisher Scientific) or NucRed Live 647 ReadyProbes (cat. R37106, Thermo Fisher Scientific) according to the manufacturers' instructions. Data was acquired on the Amnis ImageStreamX Mark II instrument (Merck Millipore). Spectral compensation, background correction and adaption of the nuclear mask was performed, and images were analyzed with the IDEAS image analysis software by calculating nuclear translocation of GFP-labeled CD93. A minimum 1200 GFP^+ cells were analyzed per sample unless otherwise specified in the Figure legends.

To address nuclear CD93 expression in human $CD34^+$ CML stem/progenitor cells and K562 and STR-4 cell lines, cells were sequentially stained after fixation and permeabilization prior to staining with αCD93 (cat. ab134079, 1:1000) and anti-rabbit IgG (H+L), F(ab')2 Fragment Alex Fluor 488 was from Cell signaling (cat. 4412, 1:1000) both diluted in DAKO diluent (cat. S0809, Dako).

Sub-cellular fractionation and Western Blot

After the FACS-sorting, K562 cells expressing pLVX-AcGFP1-N1 or pLVX-AcGFP1-N1-*Cd93* were washed twice with ice-cold PBS. The cell pellet was re-suspended in 0.1% NP40 (cat. 28324, Thermo Fisher Scientific)-PBS. An aliquot was removed as the whole cell lysate. The remaining lysate was centrifuged for 10 s. and the supernatant was transferred to a new tube as the cytoplasmic fraction. The pellet was re-suspended in ice-cold NP40-PBS followed by the centrifugation. The supernatant was discarded, and the remaining pellet was kept as a nuclear fraction. The whole cell lysate and the nuclear fraction were re-suspended in 1x Laemmli buffer (cat. 610747, Biorad) containing β- mercaptoethanol followed by sonication using microprobes 5x for 2 s. at 40% intensity. The cytoplasmic fraction was resuspended in Laemmli buffer; all samples were boiled for 5min and loaded on the 4%–20% Mini-PROTEAN® TGX Stain-Free Protein Gels (cat. 4568096, Biorad). The transfer was performed using Trans-Blot® Turbo RTA Mini PVDF Transfer Kit (cat. 1704272, Biorad). The membranes were blocked for 2h in 5% BSA and incubated overnight, at 4°C, with the following antibodies: αGFP (cat. ab290, abcam, 1:1000), α-lamin B1 (cat. Ab16048, Abcam, 1:1000) and α-alpha tubulin (DM1A) (cat. ab7291, Abcam, 1:1000). The membranes were incubated with HRP conjugated secondary antibodies: α-mouse IgG (cat. 7076, Cell signaling, 1:10000) or α-rabbit IgG (cat. 7074, Cell signaling, 1:1000). Proteins were detected with Clarity Western ECL Substrate (cat. 1705060, Biorad) and visualized on ChemiDoc Imaging Systems.

Immunohistochemistry (IHC)

IHC stainings were performed on a Leica BOND RX automated immunostainer (Leica Biosystems). Thin sections (1-2 μm) of formalin-fixed paraffin-embedded (FFPE) tissue were pre-treated by boiling at 100°C in citrate buffer, pH 6.0 for 30 min. Double stainings were performed sequentially: First, slides were stained with rabbit anti-human CD93 (polyclonal, Sigma #HPA012368; dilution 1:50) for 30 min, followed by visualization using the Bond Polymer Refine DAB Detection kit (cat. DS9800, Leica Biosystems). Then, slides were counterstained using mouse anti-human CD34 (clone QBEnd/10, Cell Marque cat. 134M-16; dilution 1:200) for 15 min, followed by visualization using the Bond Polymer Refine Red Detection kit (cat. DS9390, Leica Biosystems). Finally, the samples were counterstained with hematoxylin and mounted with Aquatex® (cat. 108562, Merck Millipore). Slides were digitized using a Pannoramic 250 Flash III scanner (3DHistech). Analysis and quantification of the stainings was performed under the supervision of a board-certified surgical pathologist (C.M.S.).

High-throughput transcriptome analysis using next generation RNA sequencing (RNA-Seq)

Total RNA was extracted from naive BL/6 and $CD93^{-/-}$ LSKs (n = 2/group) and BL/6 LSCs isolated from primary CML mice (n = 3/group) that were subjected to *in vivo* treatment with either vehicle or MCP (10mg/kg) using the RNeasy Micro Kit (cat. 74004, QIAGEN). Total RNA quality was determined by a Bioanalyzer using the RNA 6000 Nano Chip (Agilent Technologies) and quantified by fluorometry using the Quantifluor RNA System Kit (cat. E3310, Promega) on a Quantus Fluorometer Instrument (Promega).

Library preparation was performed from total RNA using the SMART-Seq v4 Ultra Low Input RNA Kit for Sequencing (Takara Bio). Libraries were quality-checked on the Fragment Analyzer using the High Sensitivity NGS Fragment Analysis Kit (Agilent). Samples were pooled to equal molarity and the pool was quantified by fluorometry, in order to be loaded at a final concentration of 2pM on the NextSeq 500 instrument (Illumina). Samples were sequenced SR76 using the NextSeq 500 High Output Kit 75-cycles (Illumina) and primary data analysis was performed using the Illumina RTA version 2.4.11 and bcl2fastq v2.20.0.422.

RNA-Seq data analysis

The RNA-Seq data was assembled by SeqMan NGen software v.15 and analyzed using ArrayStar software v.15 (DNASTAR, USA). The level of gene expression was assessed after normalization and log2 transformation. The dataset was analyzed by two-way ANOVA. Genes with significant difference in their expression at FDR-$p < 0.05$ and fold differences ≥ 1.5 were selected. Data were clustered using standard Euclidean's method based on the average linkage and heatmaps were generated according to the standard normal distribution of the values.

Gene ontology (GO) and gene set enrichment analysis (GSEA).

GO enrichment was assessed using Partek® Genomics Suite™ software, v.7 (Partek). The list of differently expressed genes was grouped into functional hierarchies. Enrichment scores were calculated using a chi-square test comparing the proportion of the gene list in a group to the proportion of the background genes. A value of 3 or higher corresponded to a significant overexpression ($p < 0.05$). GSEA was performed using GSEA software v.3.0 (Broad Institute). Enrichment analysis was assessed for all pathway-related genes acquired from pathcards database (https://pathcards.genecards.org/) and the gene sets RAMALHO_STEMNESS_UP (Ramalho-Santos, 2002) and MA_MYELOID_DIFFERENTIATION_UP (Ma et al., 2002).

qRT-PCR

Total RNA was extracted from FACS-sorted human $CD34^+$ LSCs, murine LSCs or LSKs using the RNeasy Micro Kit (cat. 74004, QIAGEN). For each sample, cDNA synthesis was assessed using High Capacity cDNA Reverse Transcription Kit (cat. 4368814, ThermoFisher). Primers were designed for each gene using Primerquest Software (Integrated DNA Technologies). For qRT-PCR analysis, synthesized cDNAs amplified with specific primers using FastStart Universal SYBR® Green 2X PCR Master Mix (cat. 04913850001, Roche). Raw values were normalized using geometric mean of reference genes (*ACTB* and *GAPDH*). Real-time PCR reactions were performed in replicates and included no-template controls using ABI Prism 7500 Sequence Detection System (Applied Biosystems). The fold difference for each sample was calculated using the comparative Ct method. The following primer pairs were used to determine mRNA expression of respective genes in human $CD34^+$ LSCs, murine LSCs or LSKs are depicted in Table S4.

CML model

FACS-purified LSKs were harvested and transduced twice with BCR-ABL1-GFP or -CFP retrovirus by spin infection at a multiplicity of infection (MOI) of 0.5. $3x10^4$ cells were injected intravenously (i.v.) into the tail vein of non-irradiated syngeneic recipients. To determine residual disease in surviving mice, CML mice were sacrificed 90 days after transplantation and $5x10^6$ BM cells were injected i.v. into lethally irradiated (2 × 6.5 Gy) recipient mice.

For MCP treatment (prophylactic setting), CML mice were treated daily once p.o. with MCP (Sigma) at a concentration of 10mg/kg (Shalaby et al., 2013) starting at the day of CML induction.

For MCP treatment (therapeutic setting), BL/6 CML mice were randomized at day 13 after leukemia induction and were treated with either vehicle or MCP (10mg/kg) for 3 days. At day 16, mice were sacrificed, and BM LSCs of individual mice were FACS-purified and subjected to RNA sequencing analysis.

LSPC and HSPC analysis

LSCP numbers in CML mice an HSCP numbers in naive mice were analyzed as described before (Riether et al., 2015b; Schürch et al., 2014).

LSC homing experiments

$5x10^4$ BL/6 or *Cd93*$^{-/-}$ LSCs were transplanted i.v. into lethally irradiated (2 × 6.5Gy) or non-irradiated BL/6 mice. 14h later mice were sacrificed, and BM was analyzed for the presence of GFP^+ LSCs.

BrdU incorporation *in vivo*

CML mice were injected i.p. with 1 mg BrdU (cat. B5002, Sigma). 14 h later, mice were sacrificed and BrdU staining was performed using the BD PharMingen BrdU Flow Kit according to the manufacturer's instructions (cat. 552598).

QUANTIFICATION AND STATISTICAL ANALYSIS

All flow cytometry, *in vitro* and *in vivo* data were analyzed and plotted using GraphPad Prism® software v7.0 (GraphPad). Bars and error bars indicate means and standard deviations of the indicated number of independent biological replicates, respectively, if not otherwise specified. Two-tailed Student's t test, one-way-ANOVA followed by Dunnett's or Tukey's post-test, two-way ANOVA followed by Bonferroni post-test were used as indicated in the legends. LSC frequencies with 95% confidence intervals (CI) were estimated with ELDA software (http://bioinf.wehi.edu.au/software/elda/) and significant differences in LSC frequency were calculated by $\chi 2$ test in limiting dilution assays according to (Hu and Smyth, 2009). Significance of differences in Kaplan-Meier survival curves was determined using the log-rank test (two-tailed). $p < 0.05$ was considered significant. Details on the quantification, normalization and statistical tests used in every experiment can be found in the corresponding figure legend. n represents the number of independent replicates in each experiment.